Effect of dry friction on a parametric nonlinear oscillator

S. Benacchio, C. Giraud-Audine, O. Thomas

Nonlinear Dynamics manuscript No.
(will be inserted by the editor)

Effect of dry friction on a parametric non linear oscillator

S. Benacchio · C. Giraud-Audine · O. Thomas

Received: date / Accepted: date

Abstract Parametrically excited oscillators are used in several domains, in particular to improve the dynamical behaviour of systems like in the case of the parametric amplification or parametric energy harvesting. Although dry friction is often omitted during system modelling due to the complexity of its non-smooth nature, it is sometimes necessary to account for this kind of damping to adequately represent the system motion. In this paper, it is proposed to investigate the effect of dry friction on the dynamical behaviour of a non linear parametric oscillator. Using the pendulum case as example, the problem is formulated according to a Mathieu-Duffing equation. Semi-analytical developments using the harmonic balance method and the method of varying amplitudes are used to find the solutions of this equation and their stability. These results are validated thanks to a comparison with time integration simulations. Effects of initial conditions on the basins of attractions of the solutions are also studied using these simulations. It is found that trivial and non trivial solutions of the oscillator including dry friction are not connected, giving birth to isolated periodic solutions branches. Thus, both initial displacement and phase between the excitation and the oscillator displacement must be carefully chosen to reach periodic solutions. Finally, a method based on the energy principle is used to find the critical forcing amplitude and frequency needed to obtain the birth of non trivial solutions for the non linear parametric oscillator including dry friction.

Keywords Parametric nonlinear oscillator · dry friction · isola · critical forcing amplitude

1 Introduction

In the context of dynamical systems, damping is often a complex issue. Although viscous damping is fairly well understood, dry friction is usually simplified or even neglected due to its nonlinear and non smooth nature. However, numerous applications exhibit a dynamical behaviour influenced by dry friction which is still the topic of a lot of studies [15, 11, 26, 32, 2, 31]. One particular

S. Benacchio
Arts et Métiers, Laboratoire d'Ingénierie des Systèmes Physiques et Numériques (LISPEN EA 7515), Lille, France.
E-mail: Simon.Benacchio@ensam.eu

C. Giraud-Audine
Univ. Lille, Arts et Metiers Institute of Technology, Centrale Lille, Junia, ULR 2697 - L2EP –F-59000 Lille, France

O. Thomas
Arts et Métiers, Laboratoire d'Ingénierie des Systèmes Physiques et Numériques (LISPEN EA 7515), Lille, France.

kind of systems which is often investigated omitting dry friction is the familly of parametrically excited systems whose dynamical behaviour is derived from Mathieu's equation [4,21,3,30,1]. As in every resonant system, parametric resonances can be a source of perturbation if uncontrolled but can also be used as an enhancement of the system dynamics like in the case of parametric amplification [24,29] or parametric energy harvesting [8,12,28].

A famous textbook case of parametrically excited systems is the parametric pendulum whose dynamical behaviour has been extensively studied in numerous references [4,3,30,33,9]. Among all the studies dealing with the parametric pendulum dynamics, some of them take into account a dry friction term in the governing equations. For example, Yabuno et al. have used a pendulum including dry friction to control the parametric resonance of a beam [34]. Gonzalez et al. have studied a coupled oscillator/pendulum system including dry friction, viscous and quadratic damping to illustrate the use of a real-time dynamical substructuring modelling method [13]. Yano proposes to study the effect of dry friction in a parametrically self-excited system [35]. The identification of viscous and Coulomb damping parameters in a parametric pendulum is addressed in [18]. Interesting contributions about viscous and dry friction damping applied to non parametric pendulum are presented in [23,5]. The general case of a parametric oscillator including dry friction is addressed in [7].

When dealing with parametrically excited systems, the existence of resonant motion depends on a critical forcing amplitude related to the damping amount. In the case of a viscously damped system, this critical forcing amplitude can be analytically derived from the existence of non zero solutions when using perturbation methods [30]. In this case, the birth of the parametric resonance occurs at the resonance frequency of the system when looking to its frequency response curves. Thus, for a system including only viscous damping, the two bifurcated branches of the non trivial solutions emerge from the branch of the trivial solutions describing the motionless equilibrium of the system. When a dry friction term is added to the governing equations, branches of non trivial solutions are not connected to the branch of trivial solutions anymore. The split between branches of trivial and non trivial solutions of the system leads to the emergence of an isola, as observed in [35] for example. It is likely that the critical forcing amplitude and the corresponding frequency leading to the birth of an isola are not the same with and without dry friction. However, it seems that no criterion can be found in the literature to obtain these forcing amplitude and frequency.

A second remark on the difference between a system with purely viscous and mixed viscous and dry friction damping is about the influence of initial conditions. Indeed, in the case of a viscously damped parametric pendulum, trivial solutions are unstable between the two aforementioned bifurcations (see [30] for example). Thus, the system necessarily jumps to the stable non trivial solution branch when perturbed in this frequency band. In the case of mixed viscous and dry friction damping, the stability of the motionless state of the system observed experimentally suggests that the trivial solution is stable for every frequency. Thus, the jump on a non trivial solution branch is not ensured but depends on the amplitude and phase of the excitation initially applied to the system. However, it remains unclear how these initial conditions have to be set to reach the stable periodic orbits of the system.

In this paper, we address two important issues when dealing with parametric non linear systems that include viscous and dry friction damping. Firstly, we propose to investigate the way initial conditions must be set to reach the stable non trivial solutions of the system. Secondly, we investigate the critical forcing amplitude and frequency for which the birth of these non trivial solutions (isola) occurs. The example of the parametrically excited pendulum is used to illustrate the aforementioned propositions. A modelling of a parametrically excited pendulum including a dry friction term is proposed. Solutions of the dynamical system are numerically approximated using the harmonic balance method formalism. Stability of trivial and non trivial

solutions is investigated using the method of varying amplitude proposed in [1]. Obtained results are compared with numerical ones computed thanks to a time integration of the dynamical system equations. In order to avoid the regularization of the dry friction term, a switch model presented in [19] is used. Then, effects of the initial conditions on the basins of attraction of the pendulum solutions are investigated thanks to time integration simulations. Finally, the critical frequency for which non trivial solutions exist is numerically computed using a method based on the energy principle [6]. The corresponding critical forcing amplitude is analytically derived from this value.

2 Governing equations

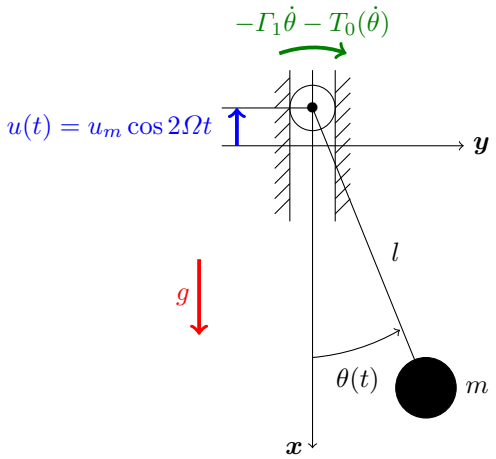

Fig. 1 A parametrically excited pendulum with viscous and dry friction.

As shown in Figure 1, we consider a pendulum parametrically excited by a vertical displacement $u(t) = u_m \cos 2\Omega t$, with u_m and 2Ω the amplitude and the angular frequency of the excitation respectively. The angular frequency deliberately appears with a factor 2 in the modelling in order to exhibit the parametric behaviour of the system occurring at twice the natural frequency in the case of the pendulum. The equation of motion for the angular displacement $\theta(t)$ of the pendulum is derived from Newton's second law and reads

$$ml^2\ddot{\theta} + \Gamma_1\dot{\theta} + T_0(\dot{\theta}) + ml[g + \ddot{u}]\sin\theta = 0, \tag{1}$$

where $\dot{\bullet}$ denotes the derivative of $\bullet$ with respect to time t. Parameters g, l and m are respectively the gravitational acceleration, le length and the mass of the pendulum. Terms $-\Gamma_1\dot{\theta}$ ($\Gamma_1 \in \mathbb{R}^+$) and $-T_0(\dot{\theta})$ correspond respectively to viscous and dry friction damping torques applied at the rotating point of the pendulum. With $\omega_0^2 = g/l$ the natural angular frequency of the conservative pendulum, Eq. (1) is rewritten such as

$$\ddot{\theta} + \mu_1\dot{\theta} + f_0(\dot{\theta}) + [\omega_0^2 + \delta\cos 2\Omega t]\sin\theta = 0, \tag{2}$$

where $\mu_1 = \Gamma_1/ml^2$ is the viscous damping coefficient. The parametric driving amplitude reads $\delta = -4\Omega^2\tilde{\delta}$, with $\tilde{\delta} = u_m/l$. This writing is useful in the case of a prescribed displacement

forcing, for which u_m is independent of Ω. In the case of a prescribed acceleration forcing $\ddot{u}(t) = a_m \cos 2\Omega t$, Eq. (2) is rewritten with an acceleration amplitude a_m independent of Ω, such as $\delta = \tilde{\delta}_a = a_m/l$. In this paper, we will mainly consider the case of a prescribed displacement. Examples of prescribed acceleration are treated in Appendix A.

The dry friction function $f_0(\dot{\theta}) = T_0(\dot{\theta})/ml^2$ is defined according to the Coulomb's law, such as

$$f_0(\dot{\theta}) \begin{cases} = \mu_0, & \dot{\theta} > 0 \quad (3a) \\ \in [-\mu_0, \mu_0], & \dot{\theta} = 0 \ , \quad (3b) \\ = -\mu_0, & \dot{\theta} < 0 \quad (3c) \end{cases}$$

where μ_0 is the dry friction coefficient [17]. Equations (3a,c) correspond to a slip phase, for which the velocity is nonzero and the friction force is piecewise constant: $f_0(\dot{\theta}) = \mu_0 \operatorname{sign}(\dot{\theta})$. Equation (3b) represents a stick phase, where the pendulum is motionless and the friction force that can take any value between $-\mu_0$ and μ_0. Notice that we consider in this paper identical slip and stick friction coefficients. Together with Eq. (3b) that is a set-valued function, the equation of motion (2) can be regarded as a differential inclusion [20]. Naturally deduced from Eqs. (3a-c), the transition from a slip phase to a stick phase occurs whenever $\dot{\theta}$ becomes zero at a given instant. On the contrary, the transition from a stick phase to a slip phase must be viewed with the associated equation of motion. We rewrite Eq. (2) as

$$\ddot{\theta} - f_{\mathrm{re}} + f_0(\dot{\theta}) = 0, \quad (4)$$

where f_{re} is the restoring force (all the forces applied to the pendulum but the inertia force and the friction force). In the stick phase, $\dot{\theta} = \ddot{\theta} = 0$ leads to $f_0(\dot{\theta}) = f_{\mathrm{re}}$ (the static version of (4)) and according to Eq. (3b), the transition from a stick phase to a slip phase occurs at an instant where $|f_{\mathrm{re}}|$ becomes larger than μ_0. In addition, according to the basic equilibrium of the pendulum, the choice of Eqs. (3a) or (3c) for the next slip phase depends on how $|f_{\mathrm{re}}| > \mu_0$: if $f_{\mathrm{re}} > \mu_0$ (resp. $f_{\mathrm{re}} < -\mu_0$), the next slip phase is governed by Eqs. (3a) (resp. Eq. (3c)).

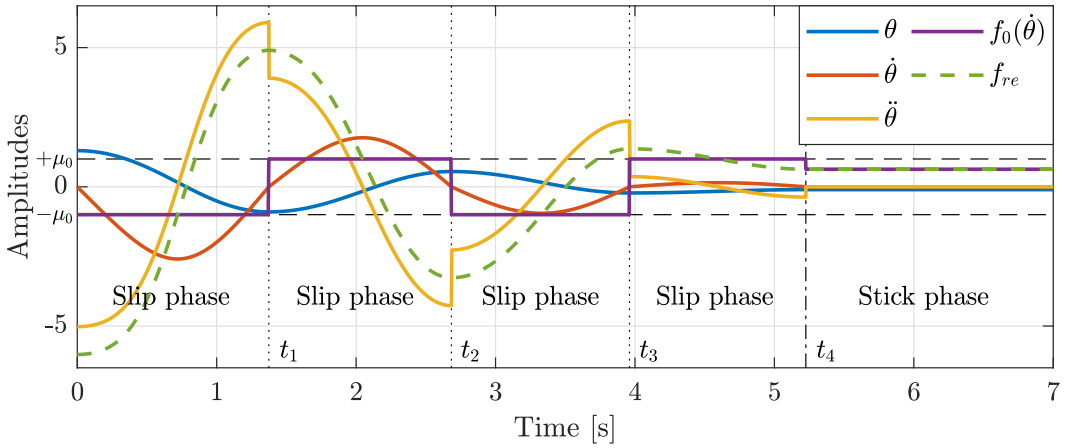

Fig. 2 Time evolution results for the free oscilations of the pendulum without viscous damping ($\mu_0 = 1$, $\delta = 0$) with $\omega_0 = 2.5$ and $\mu_1 = 0$. Initial conditions in position and velocity are respectively $\theta_0 = 1.3$ rad and $\dot{\theta}_0 = 0$ rad/s. The curves corresponds to angle $\theta(t)$, velocity $\dot{\theta}(t)$, acceleration $\ddot{\theta}(t)$, restoring force $f_{\mathrm{re}}(t)$ and of friction force $f_0(\dot{\theta}(t))$.

To give an example of the dry friction effect on the pendulum behaviour studied in this article, we consider Eq. (2) in free oscillations with no viscous damping ($\delta = \mu_1 = 0$), such as $f_{\text{re}} = -\omega_0^2 \sin\theta$. Results of the motion of the pendulum, according the time integration algorithm presented in Section 4.2, are shown in Figure 2. Blue, red and yellow curves correspond to the angular displacement, velocity and acceleration respectively. Purple curve is the dry friction force $f_0(\dot{\theta})$ and the green dashed curve is the restoring force f_{re} applied to the pendulum. According to Eq. (4), the difference between the green and purple curves must always be equal to the yellow curve. Horizontal dashed lines correspond to $\pm$ the value of the dry friction coefficient μ_0. The description of the pendulum motion affected by the dry friction force can be done as follow. For $t = 0$, $\dot{\theta} = 0$ and $|f_{\text{re}}| > \mu_0$ with $f_{\text{re}} < -\mu_0$. In these conditions, the system is in a slip phase until $\dot{\theta} = 0$, at $t = t_1$. At this instant, $|f_{\text{re}}| > \mu_0$ with $f_{\text{re}} > \mu_0$, which changes the sign of $f_0(\dot{\theta})$ with respect to the previous slip phase, during a stick phase of zero duration. This behaviour continues until $t = t_4$. At this instant, $\dot{\theta} = 0$ but with $|f_{\text{re}}| < \mu_0$. In these conditions, the pendulum falls in a final stick phase, since its restoring force is included in a dead-zone delimited by $\pm\mu_0$ in which it is not large enough to overcome the dry friction force. Thus, the motion of the pendulum is a succession of slip phases terminated by a stick phase. In the remaining of the paper, we will consider steady state periodic motion of parametric oscillators and we will assume the same behaviours: either a succession of slip phases or a final stick phase if $|f_{\text{re}}| < \mu_0$ is in the dead-zone.

Regarding Eq. (2), one can use the approximation $\sin\theta \approx \theta - \frac{1}{6}\theta^3$ for finite and not too large oscillations. With in mind the use of a perturbation method to calculate the approximated solutions of the angular displacement of the pendulum, the multiplication between the excitation term $\delta\cos 2\Omega t$ and the third-order term $-\frac{1}{6}\theta^3$ is neglected, resulting in

$$\ddot{\theta} + \mu_1\dot{\theta} + f_0(\dot{\theta}) + [\omega_0^2 + \delta\cos 2\Omega t]\theta - \gamma\theta^3 = 0. \tag{5}$$

In order to remain in a general frame, the nonlinear coefficient $\gamma = \omega_0^2\tilde{\gamma}$ is introduced in Eq. (5) and not restricted to the pendulum case ($\tilde{\gamma} = 1/6$) in the following section. Thus, the governing Eq. (5) is extended to a Mathieu-Duffing problem type. It is also worth mentioning that the behaviour of the system depends on only three free parameters, related to μ_1, μ_0 and δ. This can be proven with a dimensionless rewriting of Eq. (5) with time and angle scaling, as shown in Appendix B. Consequently, in the remaining of the paper, without loss of generality, only the variations of those three parameters will be considered in the investigations.

3 Analytical developments

In this section, we seek an analytical solution of Eq. (5) with a perturbation method. We use the method of varying amplitude (MVA) proposed in [27] and used in [1]. This method is very close to the harmonic balance method (HBM), the difference being that in the MVA we allow the amplitude of the harmonic components to be time varying, in order to access to a stability analysis. We us this method here, in comparison to more standard ones such as the method of multiple scales [22], because it gives results closer to the numerical reference solution in the present case of parametric resonances (see Appendix A for details).

3.1 Method of varying amplitude

In this section, the motion of a nonlinear parametric oscillator described by Eq. (5) is studied. Following the MVA formalism, the Equation of motion (5) is rewritten using a Fourier series

expansion of the angular displacement with only one harmonic such as

$$\theta(t) = a(t)\cos\Phi(t), \quad \Phi(t) = \Omega t + \beta(t), \tag{6}$$

with $a(t)$ the amplitude and $\beta(t)$ the phase of the angular displacement single term expansion. Although the amplitude/phase formalism is convenient for calculation, the Cartesian form of the angular displacement will be needed for the upcoming stability study and writes

$$\theta(t) = A_1(t)\cos\Omega t + B_1(t)\sin\Omega t, \tag{7}$$

with

$$A_1(t) = a(t)\cos\beta(t), \quad B_1(t) = -a(t)\sin\beta(t). \tag{8}$$

The dry friction term is also expanded using a one term Fourier series such as

$$f_0(\dot\theta) = f_{c1}\cos\Phi + f_{s1}\sin\Phi = F_{c1}\cos\Omega t + F_{s1}\sin\Omega t \tag{9}$$

with f_{c1}, f_{s1} and F_{c1}, F_{s1} the coefficients of the expansion in the Φ and Ωt form respectively. Unlike the coefficients of the angular displacement expansion, the coefficients of Eq. (9) are assumed to be constant since it is not possible to analytically compute their derivatives used to find the stability of the system otherwise (see Section 3.2). This approximation will be validated with comparison to a numerical solution in Section 4.

Injecting (6) and (9) in (5), grouping terms by harmonics and considering only the first harmonic in Φ (see Appendix C for details), results in

$$\begin{cases} \ddot a - a\,(\Omega+\dot\beta)^2 + \dot a\,\mu_1 + a\omega_0^2 + f_{c1} + \dfrac{1}{2}\,a\,\delta\,\cos 2\beta - \dfrac{3}{4}\,a^3\,\gamma = 0 & \text{(10a)} \\ -2\,\dot a\,(\Omega+\dot\beta) - a\,\ddot\beta - a\,\mu_1\,(\Omega+\dot\beta) + f_{s1} + \dfrac{1}{2}\,a\,\delta\sin 2\beta = 0 & \text{(10b)} \end{cases}$$

where Equations (10a) and (10b) are obtained equating to zero the coefficients of $\cos\Phi$ and $\sin\Phi$ respectively.

To find the fixed points of the system, all time derivatives are set to zero ($\ddot a = \ddot\beta = \dot a = \dot\beta = 0$). Under these conditions, Equations (10) are similar to those obtained with a usual harmonic balance method. Since only slip phases are considered here, the friction term Fourier coefficients are computed multiplying $f_0(\dot\theta) = \mu_0\ \mathrm{sign}(\dot\theta)$ with the corresponding trigonometric function ($\cos\Omega t$ or $\sin\Omega t$) and integrating over one period of the displacement motion. These coefficients read

$$\begin{cases} f_{c1} = 0 \\ f_{s1} = -\frac{4\mu_0}{\pi} \end{cases} \tag{11}$$

In these conditions, Equations (10) result in

$$\begin{cases} a\omega_0^2 - a\Omega^2 - \dfrac{3}{4}a^3\,\gamma + \dfrac{1}{2}a\delta\cos 2\beta = 0 & \text{(12a)} \\ -a\mu_1\Omega - \dfrac{4\mu_0}{\pi} + \dfrac{1}{2}a\delta\sin 2\beta = 0 & \text{(12b)} \end{cases}$$

It is noteworthy that the trivial case $a = 0$ (corresponding to a stick phase) is not a solution of the System of equations (12) when $\mu_0 \neq 0$. This motionless case is discussed in Section 3.3.

Eliminating 2β in Equations (12) to find the amplitude a results in the 6^{th} degree polynomial equation

$$\frac{9}{16}\gamma^2 a^6 - \frac{3}{2}\gamma(\omega_0^2 - \Omega^2)a^4 + \left[(\omega_0^2 - \Omega^2)^2 + \Omega^2\mu_1^2 - \frac{1}{4}\delta^2\right]a^2 + \frac{8}{\pi}\Omega\mu_0\mu_1 a + \frac{16}{\pi^2}\mu_0^2 = 0. \quad (13)$$

When solving Eqs. (12) in β, one finds

$$\tan(2\beta) = \frac{\Omega\mu_1\, a + \frac{4}{\pi}\mu_0}{\frac{3}{4}\gamma a^3 - (\omega_0^2 - \Omega^2)a} \quad (14)$$

3.2 Stability

The stability of solutions is investigated injecting the Cartesian form given by Eq. (7) in Eq. (5) Equating the terms in $\cos\Omega t$ and $\sin\Omega t$ with zero results in a system of two second order equations which can be rewritten at first order using $A_2 = \dot{A}_1$ and $B_2 = \dot{B}_1$ and reads

$$\begin{cases} \dot{A}_1 = A_2 \\ \dot{A}_2 = (\Omega^2 - \omega_0^2)A_1 - \mu_1 A_2 - \mu_1\Omega B_1 - 2\Omega B_2 - F_{c1} - \frac{1}{2}\delta A_1 + \frac{3}{4}\gamma A_1(A_1^2 + B_1^2) \\ \dot{B}_1 = B_2 \\ \dot{B}_2 = (\Omega^2 - \omega_0^2)B_1 - \mu_1 B_2 + \mu_1\Omega A_1 + 2\Omega A_2 - F_{s1} + \frac{1}{2}\delta B_1 + \frac{3}{4}\gamma B_1(A_1^2 + B_1^2) \end{cases} \quad (15)$$

where the friction term coefficients F_{c1} and F_{s1} are defined in Eq. (9). The Jacobian determinant of the System (15) is calculated and reads

$$\begin{aligned} \mathcal{J} = &\left[\tfrac{3}{2}\gamma A_1 B_1 - \Omega\mu_1\right]\left[\tfrac{3}{2}\gamma A_1 B_1 + \Omega\mu_1\right] \\ &- \left[(\Omega^2 - \omega_0^2) - \tfrac{\delta}{2} + \tfrac{3}{4}\gamma(3A_1^2 + B_1^2)\right]\left[(\Omega^2 - \omega_0^2) + \tfrac{\delta}{2} + \tfrac{3}{4}\gamma(A_1^2 + 3B_1^2)\right] \end{aligned} \quad (16)$$

The stability of the solutions of Eq. (13) is evaluated by numerically computing the eigenvalues of the Jacobian matrix for a given fixed point, obtained by numerically solving (13), (14) and using (8). Solutions are stable when the real part of the determinant roots are all negative and unstable otherwise. It is noteworthy that the friction term coefficients are not directly included in $\mathcal{J}$ but has an effect on the stability since the amplitudes (A_1, B_1) of the fixed points depend on μ_0.

3.3 Particular solutions

3.3.1 Trivial solutions ($a = 0$)

Because of the dry friction model, the equation of motion (4) has a trivial solution associated to a permanent stick phase. Considering a motionless state ($\dot{\theta} = \ddot{\theta} = 0$) with Eq. (3b), one shows that a value θ_{tr} of θ, defined by $f_{\text{re}}(\theta_{\text{tr}}) \in [-\mu_0, \mu_0]$, related to the dead-zone, is solution of the equation of motion (4). As mentioned in Section 2, this trivial solution as well as its stability is not predicted by the analytical developments presented in Section 3.1. This is natural since no constant component is considered in the Fourier Series expansion of Eq. (6). Adding this constant component would complicate the analytical developments and is thus not considered in the present article. The existence and stability of this trivial solution will however be studied, using time integration only, as described in Section 4.2.

3.3.2 Conservative solutions ($\mu_1 = \mu_0 = \delta = 0$)

Conservative solutions of the system in free vibrations, given by Eq. (12a) when $\mu_1 = \mu_0 = \delta = 0$, read

$$\theta_\mathrm{c} = a_\mathrm{c} \cos \Omega t \tag{17}$$

with

$$a_\mathrm{c}^2 = \frac{4}{3\gamma} (\omega_0^2 - \Omega^2) \tag{18}$$

In the amplitude/forcing frequency plane, $a_\mathrm{c} = f(\Omega)$ corresponds to the well-known backbone curve of the nonlinear oscillator, whose hardening and softening behaviour depends on the sign of the nonlinear coefficient γ.

3.3.3 Solutions with viscous ($\mu_1 \neq 0$) but no dry friction ($\mu_0 = 0$)

When there is no dry friction, analytical solutions of the amplitude and phase of the displacement can be derived from Eq. (13). In this case, the amplitude and phase read

$$a^2 = \frac{4}{3\gamma} \left((\omega_0^2 - \Omega^2) \pm \sqrt{\frac{\delta^2}{4} - \mu_1^2 \Omega^2} \right) \tag{19}$$

$$\tan(2\beta) = \pm \frac{\Omega \ \mu_1}{\sqrt{\frac{\delta^2}{4} - \mu_1^2 \Omega^2}} \tag{20}$$

Eq. (19) is the same as Eq. (18) in addition to plus or minus a term depending on the damping and forcing. Thus, the solutions are spread around the backbone curve given by Eq. (18). Moreover, the existence of a real solution is possible only if the term inside the square root is positive. This gives a criterion to find the critical forcing amplitude needed to initiate the system motion which occurs at $\Omega = \omega_0$. When the excitation is a constant forcing displacement ($\delta = -4\Omega^2\tilde{\delta}$), the critical forcing amplitude is

$$\tilde{\delta}_{\mathrm{cr},(\mu_0=0)} = \frac{\mu_1}{2\omega_0}. \tag{21}$$

When the excitation is a constant forcing acceleration ($\delta = \tilde{\delta}_a$), the critical forcing amplitude is

$$\tilde{\delta}_{a,\mathrm{cr},(\mu_0=0)} = 2\mu_1\omega_0. \tag{22}$$

3.4 Theoretical frequency responses for representative cases

To depict the behaviour of the system in representative cases, the example of a pendulum ($\tilde{\gamma} = 1/6$), having a unit resonance angular frequency ($\omega_0 = 1$) and excited with a constant forcing displacement ($\delta = -4\,\Omega^2\,\tilde{\delta}$) is used. As explained in Appendix B, the qualitative behaviour of the system is independent of ω_0 and depends on the sign of γ, which results in a hardening or softening behaviour, and not on its absolute value. We treat here only the case of a softening behaviour ($\gamma > 0$). Other cases (hardening behaviour and prescribed acceleration driving) are partially treated in section A. The solutions of Eq. (13) are numerically computed using the *roots* algorithm in Matlab[1] and plotted in Figure 3 for several forcing amplitudes ($\tilde{\delta}$), viscous and dry friction damping (μ_1, μ_0).

[1] The roots of the polynomial are computed as the eigenvalues of the companion matrix of the polynomial

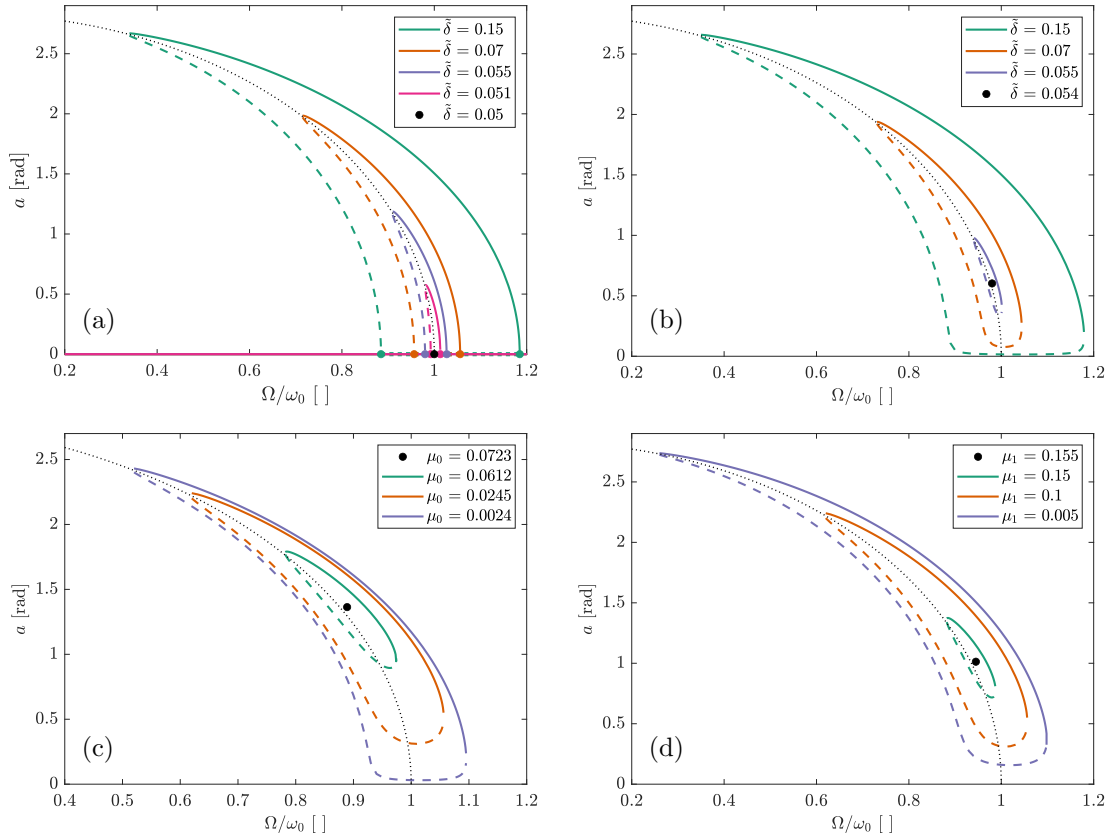

Fig. 3 Amplitude of the first harmonic of the parametric pendulum motion for several representative cases of forcing amplitude, viscous and dry friction damping. (a) $\mu_0 = 0$, $\mu_1 = 0.1$ and $\tilde{\delta} = [0.051, 0.055, 0.07, 0.15]$, (b) $\mu_0 = 0.0024$, $\mu_1 = 0.1$ and $\tilde{\delta} = [0.051, 0.055, 0.07, 0.15]$, (c) $\mu_0 = [0.0024, 0.0245, 0.0612]$, $\mu_1 = 0.1$ and $\tilde{\delta} = 0.1$, (d) $\mu_0 = 0.0245$, $\mu_1 = [0.005, 0.1, 0.15]$ and $\tilde{\delta} = 0.1$. Plain and dashed lines correspond respectively to stable and unstable solutions. Black dotted lines show the backbone curve corresponding to the conservative solution (see Eq. (18)) and the black bullets show the isola birth location for (a) $\tilde{\delta}_{\mathrm{cr},(\mu_0=0)} = 0.050$, (b) $\tilde{\delta}_{\mathrm{cr}} = 0.054$, (c) $\mu_0 = 0.0723$ and (d) $\mu_1 = 0.155$. Coloured bullets in Figure 3(a) correspond to the bifurcation points between trivial and non trivial solutions.

Figure 3(a) presents the results of the parametric pendulum amplitude with no dry friction as described by Eq. (19). In this case, the trivial solution $a = 0$ is predicted by the theoretical development of Section 3.1 and always exists. The birth of the parametric resonance is depicted with the black bullet in Figure 3(a) and emerges at the resonance angular frequency of the pendulum (for $\Omega = \omega_0$) when the forcing amplitude overcomes the critical forcing amplitude value given by Eq. (21). In this case, the numerical computation of the solutions stability given by the MVA approach leads to unstable trivial solutions between the two bifurcation points represented by coloured bullets. The upper and lower branches of the non trivial solutions are respectively stable and unstable. When increasing the forcing amplitude, the non trivial solutions grow around the backbone curve described by Eq. (18).

In Figure 3(b), a dry friction term is added to the governing equation of the pendulum with $\mu_0 = 0.0024$. As explained in section 3.3.1, the stick state resulting from Eq. (3b) is not predicted by Eq. (13). However, this static state is studied in Section 4 using time integration simulations and reveals that trivial solutions always exist. Therefore, non trivial solutions are disconnected

from the trivial solutions giving birth to an isola. When increasing the forcing amplitude, the isola emerges from a non zero amplitude depicted by the black bullet and grows around the backbone curve. The birth of the isola has been manually found decreasing the forcing amplitude until only one non trivial solution remains on the entire frequency band. It appears that the birth of the isola does not occur at the resonance angular frequency of the pendulum but slightly lower and not exactly on the backbone curve. The comparison between 3(a) and 3(b) also shows that the critical forcing amplitude is larger with dry friction.

Figure 3(c) presents the effect of μ_0 on the solutions of Eq. (13). As usually with damping terms, the larger the coefficients are, the more damped the solution is. Again, the dry friction coefficient has an effect on the location of the isola birth depicted by the black bullet. It changes the critical forcing amplitude and angular frequency of the system. Since the isola birth does not occur exactly on the backbone curve, isolated non trivial solutions which never cross the backbone curve might exit according to the analytical developments proposed in Section 3.1. Such a case is further studied in Section 4.3. Figure 3(d) presents the effect of μ_1 on the non trivial solutions and reveals similar conclusions.

4 Numerical validation of the analytical developments

Time integration simulations are used to (i) validate the existence and the stability of the non trivial solutions computed with the MVA and presented in Section 3.1, (ii) verify the existence of trivial solutions and study their stability and (iii) investigate the effect of initial conditions on basins of attraction of trivial and non trivial solutions (see Section 5). These time integrations bring no approximations to the model and provide solutions accurate up to the numerical tolerance. For this reason, they are considered as a reference in the present paper. The simulations are performed using the *ode45* solver from the software Matlab [25]. This solver has been chosen since it is the most versatile and validated since no convergence error were noticed during computations.

4.1 Algorithm for time integration simulations with dry friction

According to Eq. (3), dry friction brings discontinuities in the restoring force of the pendulum. Since the *ode45* solver is not adapted to non-smooth differential equations, the switch model formulation proposed in [19] is used to account for the dry friction term avoiding its regularization. Each time the system switches from one phase (slip or stick) to another, the dry friction force $f_0(\dot{\theta})$ is computed according to the Coulomb's law (3) and respectively to the first and second Newton's laws when the system is in a stick and slip phase. To enable the system to quit the dead-zone defined in Section 2, when the restoring force overcomes the necessary threshold, a transition phase is added to the algorithm. Rewriting the complete equation of motion (5) with the formalism of Eq. (4), with $f_{\mathrm{re}} = -\mu_1\dot{\theta} - (\omega_0^2 + \delta\cos 2\Omega t)\theta + \gamma\theta^3$ the restoring force, the switch model of Algorithm 1 enables to compute the dry friction force $f_0(\dot{\theta})$.

The small parameter η is used to define a narrow band in which the velocity of the pendulum is considered as null. This finite band of zero velocity is necessary since it is unlikely that an exact zero value is numerically computed by the solver. In this study, this parameter is defined such as $\eta = 10^{-6}$. Details on the three possible states of the algorithm are:

- when the angular velocity is non zero ($|\dot{\theta}| > \eta$), the system is in a slip phase and the equation of motion is (5) with $f_0(\dot{\theta}) = \mu_0\,\mathrm{sign}(\dot{\theta})$;

if $|\dot{\theta}| > \eta$ **then**

$f_0(\dot{\theta}) = \mu_0 \text{ sign}(\dot{\theta})$ Slip phase (dynamical)

else if $|f_{re}| > \mu_0$ **then**

$f_0(\dot{\theta}) = \mu_0 \text{ sign}(f_{\text{re}})$ Stick to slip transition

else

$f_0(\dot{\theta}) = f_{\text{re}}$ Stick phase (static)

end

Algorithm 1: Switch model algorithm [19].

- when the angular velocity is considered as null ($|\dot{\theta}| \leq \eta$) and $|f_{\text{re}}|$ is lower than or equal to μ_0, the pendulum is in a stick phase. The pendulum is in a static state since the friction term perfectly balances the restoring force ($f_0(\dot{\theta}) = f_{\text{re}}$ in Eq. (4) leads to $\ddot{\theta} = \dot{\theta} = 0$);
- when the angular velocity is zero and $|f_{\text{re}}|$ is larger than μ_0, the pendulum passes through a transition from stick (or slip) to slip phase.

4.2 Time integration simulations

Time integrations are first used to obtain frequency responses of the parametric pendulum. For this, discrete forward and backward frequency sweeps are performed using constant frequency steps. For each step, the initial conditions are chosen equal to the final state of the previous step, in order to manage the multivalued parts of the frequency response. Precisely, the initial time angular displacement and velocity computed for step $i+1$ ($i \in \mathbb{N}^*$) are $\theta_{i+1}(0) = \theta_i(t_{\text{e}})$ and $\dot{\theta}_{i+1}(0) = \dot{\theta}_i(t_{\text{e}})$ where t_{e} is the duration of step i. Moreover, t_{e} is chosen equal to an integer number N of excitation periods ($t_{\text{e}} = 2\pi N/\Omega$), in order to avoid discontinuities in the forcing signal from one step to the next one. N is chosen large enough to reach the steady state at each step, *i.e.* when the amplitude of the last 20 periods of the simulated signal has a standard deviation lower than 0.2% of the average amplitude computed for all these periods. For each of the 20 periods, the aforementioned amplitude corresponds to the first harmonic amplitude of the expansion in Fourier series of the signal computed using a synchronous demodulation method (see [10] for example).

To obtain the frequency response of a parametric pendulum without dry friction, the initial conditions of the very first step $\theta_1(0)$ and $\dot{\theta}_1(0)$ can be set to zero since the upper branch of non trivial solutions is necessarily reached in the unstable frequency range of the trivial solutions. For a parametric pendulum including dry friction, trivial and non trivial solutions are disconnected. Therefore, two sets of initial conditions are used to follow each group of solutions.

To jump on the stable non trivial solution branch of the system, the initial conditions are set such as the first step of time integration for the forward frequency sweep is computed at $\Omega = \omega_0$ using a zero initial velocity $\dot{\theta}_1(0) = 0$ and an initial angular displacement $\theta_1(0)$ equals to the maximum theoretical value of the non trivial solutions computed with Eq. (13) at ω_0. Notice that the initial displacement must sometimes be adjusted around the computed value to initiate the motion in the basin of attraction of the stable non trivial solution branch of the system (see Figure 5 for example). The next steps of the forward sweep are computed as mentioned earlier. Then, a backward frequency sweep is computed from the same initial frequency step ($\Omega = \omega_0$)

and the results of both forward and backward sweeps are merged together to obtain the entire non trivial solution branch of the system.

To investigate the existence and the stability of the trivial solutions, a frequency sweep is performed using the same initial conditions for each step i, starting from the lowest or highest studied frequency. The initial velocity is set to zero ($\dot{\theta}_i(0) = 0$) and the value of the initial angular displacement $\theta_i(0)$ is set small enough to ensure that the system starts from a position slightly greater than the boundaries of the dead-zone (*i.e.* with $|f_{\mathrm{re}}| = \mu_0 + \epsilon$, where ϵ is a small positive parameter). Since the trivial solutions are assumed to be always stable, the system should fall in the dead-zone on the entire frequency band when excited in these conditions.

4.3 Results

The results of the time integration simulations used to validate the analytical solutions and investigate the trivial solutions existence are presented in Figure 4. These results are also useful to assess the stability of both trivial and non trivial solutions, since time integration simulations only compute the stable solutions of the system.

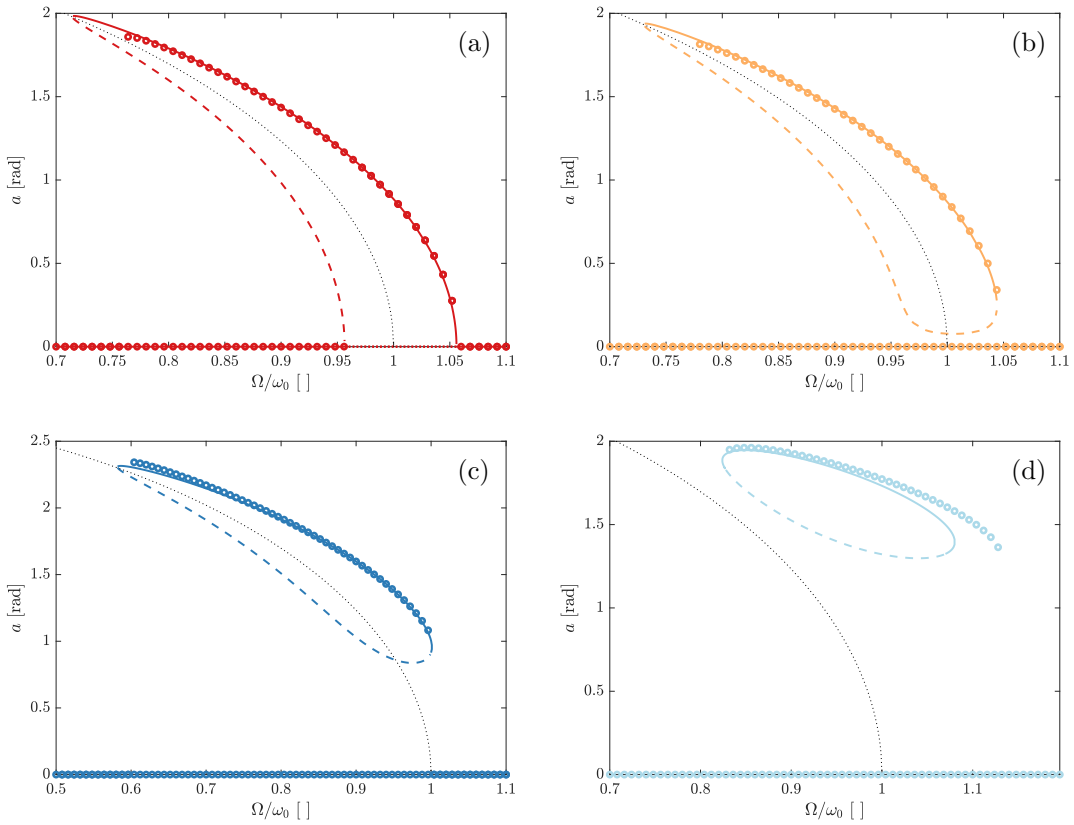

Fig. 4 First harmonic amplitude of the parametric pendulum computed using time integration simulations (circles) and compared to solutions of Eq. (13) (plain and dashed lines) for (a) $\tilde{\delta} = 0.07$, $\mu_1 = 0.1$ and $\mu_0 = 0$, (b) $\tilde{\delta} = 0.07$, $\mu_1 = 0.1$ and $\mu_0 = 0.0024$, (c) $\tilde{\delta} = 0.1$, $\mu_1 = 0$ and $\mu_0 = 0.1225$ and (d) $\tilde{\delta} = 0.26$, $\mu_1 = 0$ and $\mu_0 = 0.4899$. For all cases, $\omega_0 = 1$ and $\tilde{\gamma} = 1/6$.

Figure 4 shows that the solutions computed with the MVA (plain lines) and time integration simulations (circles) are very similar. Without dry friction (Fig. 4(a)), the trivial solutions are unstable between the two bifurcation points with the non trivial solutions. At the top of non trivial solution branches, the MVA predicts the existence of solutions a little bit higher in amplitude than time integration. This is due to the fact that only one harmonic is considered in the MVA computation. A calculation with two harmonics could be used to improve the accuracy of the results either by analytical computations as in [1] or using an asymptotic numerical method combined with harmonic balance as in [14] for example. This is left for future contributions.

Figures 4(b) and 4(c) present two cases with dry friction. The time integration simulations not only reveal that the trivial solutions always exist in this case but also that they are always stable. Indeed, even when perturbed, trivial solution persists for the entire frequency band.

Figure 4(d) presents a case with large dry friction coefficient and forcing amplitude. For this particular case, the isola does not cross the backbone curve. Compared to the time integration solutions, the MVA predicts well the non trivial solution amplitude close to the backbone but is less accurate far from the conservative solutions. However, both method predict that the non trivial solutions are disconnected form the backbone curve of the pendulum.

It is noteworthy that the amplitude of the trivial solutions presented in Figure 4(b), (c) and (d) always equals zero since it corresponds to the amplitude of the first harmonic of the simulated signal. When looking at the time signal of these simulations, the constant angular displacement reached when the velocity comes to zero is not necessarily null but is included in the dead-zone which depends on the value of the dry friction coefficient.

5 Effects of initial conditions on the basins of attraction of solutions

As observed in Figures 4(b), (c) and (d), trivial solutions of a system including dry friction are stable on the whole frequency band. To jump on a stable periodic solution branch, the critical forcing amplitude of the system must be overcome and initial conditions must be chosen carefully. Thus, a panel of initial conditions is tested using time integration simulations to obtain the basins of attraction of trivial and non trivial solutions. In this paper, it is chosen to keep the initial velocity such as $\dot{\theta}(0) = 0$ rad/s, to vary the initial displacement such as $\theta(0) \in [0, 2.2]$ rad and to test these initial conditions on a frequency band around the resonance of the system. We make this choice since in real experiments, initial conditions in term of non zero displacement with zero initial velocity are easy to be prescribed. It is worth mentioning that the maximal initial displacement corresponds to a maximal physical angle equal to 126°. This condition does not fulfil the small angle assumption made in Section 2. However, results are still relevant for the case of the Mathieu-Duffing problem given by Eq. (5), but are not computed for higher values of initial displacement since time integration simulations can diverge when $\theta(0)$ is close to 180°.

The way the forcing excites the system at $t = 0$ also affects the way the system answers to this excitation. In other words, the initial displacement of the excitation signal (bottom or top position of $u(0)$ in Figure 1 for example) has an effect on the transient displacement of the oscillator and thus, on its steady state. Therefore, the initial phase between $u(t)$ and $\theta(t)$ can change the basins of attraction of the system. In order to evaluate the effect of this initial phase, a term ϕ_0 is added to the excitation signal such as the parametric term in Eq. (5) reads $\delta \cos(2\Omega t + \phi_0)$. Several values of this phase are tested for one forcing amplitude $\tilde{\delta} = 0.07$ and one viscous damping coefficient $\mu_1 = 0.1$. For the dry friction coefficient, two cases are studied: a case without dry friction ($\mu_0 = 0$), denoted as NDF and a case with dry friction ($\mu_0 = 0.0024$), denoted as DF. These two cases correspond to time integrations presented in Figures 4(a) and

4(b) respectively. The basins of attraction obtained with time integration simulations and drawn in the $(\theta(0), \Omega/\omega_0)$ plane are presented in Figure 5.

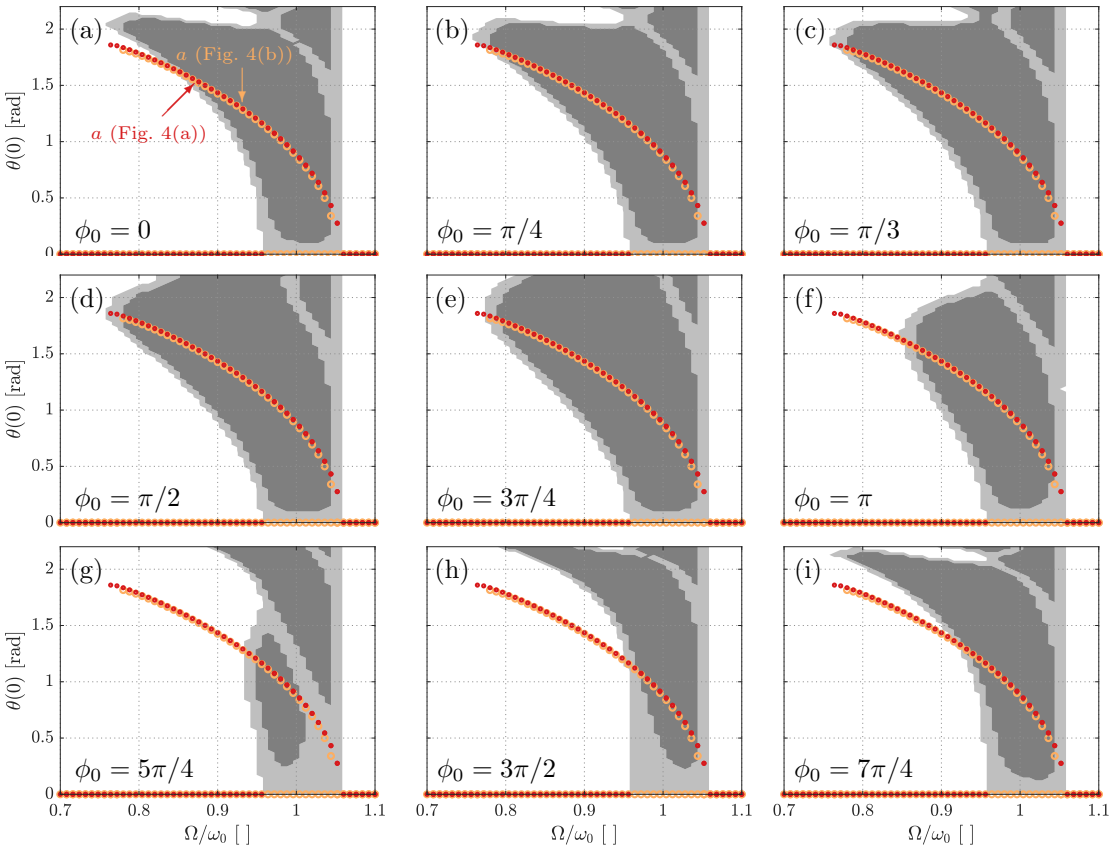

Fig. 5 Basins of attraction for non trivial solutions of Eq. (13), in the NDF case ($\mu_0 = 0$, light and dark gray) and DF case ($\mu_0 = 0.0024$, dark gray), with $\tilde{\delta} = 0.07$ and $\mu_1 = 0.1$ and for different initial phases: (a) $\phi_0 = 0$, (b) $\phi_0 = \pi/4$, (c) $\phi_0 = \pi/3$, (d) $\phi_0 = \pi/2$, (e) $\phi_0 = 3\pi/4$, (f) $\phi_0 = \pi$, (g) $\phi_0 = 5\pi/4$, (h) $\phi_0 = 3\pi/2$ and (i) $\phi_0 = 7\pi/4$. Initial angular displacement and velocity are arbitrarily chosen such as $\theta(0) \in [0, 2.2]$ rad and $\dot{\theta}(0) = 0$ rad/s. Coloured circles correspond to time integration solutions presented in Figures 4(a) (red) and 4(b) (orange).

The steady state solutions presented in Figures 4(a) and (b), corresponding to the NDF (red) and DF (orange) cases, are also plotted in Figure 5. Remark that these solutions do not depend on ϕ_0 and are thus identical on all the nine plots of Figure 5. For the DF case, the dark gray regions are the basins of attraction of non trivial solutions, represented by orange circles with a non zero amplitude. For the NDF case, the unions of dark and light gray regions are the basins of attraction of non trivial solutions, represented by red circles with a non zero amplitude. Figures 5(a) to (i) shows the effect of several initial phase ϕ_0.

The first remark about these results is that the basins of attraction for the non trivial solutions of the DF case are always included in those those of the NDF case. For the latter, the trivial solutions are always unstable between the two bifurcation points surrounding $\Omega = \omega_0$. Thus, the upper branch of non trivial solutions are systematically reached when the system is perturbed in this frequency range. For the DF case, trivial solutions are always stable. In this case and for a given forcing amplitude, the initial angular displacement must exceed a threshold value to allow

the system to jump on the branch of stable non trivial solutions. According to Figures 5(a) to (i), this threshold varies with the value of the initial phase ϕ_0.

Figure 5 also shows that the basins of attraction for non trivial solutions can be greatly reduced when ϕ_0 varies. For both DF and NDF cases, the largest basin of attraction for non trivial solutions occurs for $\phi_0 = \pi/2$. In these conditions, the system can jump on the upper branch of non trivial solutions for any frequency as long as the solution exists. The smallest basin of attraction for non trivial solutions occurs at $\phi_0 = 5\pi/4$. Obviously, the evolution of the basins of attraction with the initial phase is repeated when $\phi_0 < 0$ or $\phi_0 \geq 2\pi$. These results show that the initial displacement and phase must be carefully chosen to ensure oscillations of a system including dry friction.

6 Estimation of the critical forcing amplitude and angular frequency

Results of Section 3 can be used to compute the amplitude and phase of the motion of a parametric nonlinear oscillator for given parameters. However, it remains difficult to know what is the critical forcing amplitude $\tilde{\delta}_{\rm cr}$ needed to ensure the motion of the pendulum when dry friction is added to the system. The following section proposes to use the approach based on an energy principle method and presented in [6] to estimate this forcing threshold.

6.1 Analysis based on the energy principle

The aim of the method proposed in [6] is to find the existence of periodic solutions branches of a forced/damped system in the vicinity of a branch of free solution of the associated conservative system. For this, we first consider the quantity

$$Q[\theta, \dot{\theta}, \tau] = -\,\delta \cos 2\Omega\tau\, \theta - \mu_1\, \dot{\theta} - f_0(\dot{\theta}) \tag{23}$$

that gathers the dissipation and forcing terms of Eq. (5), as *a perturbation* of the conservative part of the equation, whose solution is denoted by $\theta_{\rm c}(t)$ (an analytical expression of $\theta_{\rm c}$ is given by Eq. (17)). For any T-periodic solution $\theta_{\rm p}(t)$ of Eq. (5) (obtained in the steady state), the work $\mathcal{W}$ of the perturbation Q over one period of the motion is necessarily null [16,6]:

$$\mathcal{W} = \int_0^T \dot{\theta}_{\rm p}(\tau)\, Q[\theta_{\rm p}(\tau), \dot{\theta}_{\rm p}(\tau), \tau]\, d\tau = 0. \tag{24}$$

This comes from Eq. (5) in which the work of the conservative part is by definition zero over one period T of the motion[2]. This result is denoted in [6] as "energy principle".

It is shown in [6] that, if we consider Q as a small perturbation of the conservative part of the equation of motion (5), the leading-order term of a Taylor expansion of Eq. (24) centred at $\theta_{\rm c}$ corresponds to the Melnikov function defined as

$$M^{1:2}(t) = \int_0^T \dot{\theta}_{\rm c}(\tau + t)\, Q[\theta_{\rm c}(\tau + t), \dot{\theta}_{\rm c}(\tau + t), \tau]\, d\tau. \tag{25}$$

This function corresponds to the energy injected and dissipated along one period of the free conservative solution $\theta_{\rm c}$, due to forcing and damping forces. The Melnikov function exponent 1:2

[2] To prove this, Eq. (5) must be multiplied by $\dot{\theta}$. Then, the conservative part is equal to the time derivative of the Hamiltonian $\mathcal{H}[\theta, \dot{\theta}] = \dot{\theta}^2/2 + \omega_0^2\theta^2/2 - \gamma\theta^4/4$, whose integral over one period gives $\mathcal{H}[\theta(T + t), \dot{\theta}(T + t)] - \mathcal{H}[\theta(t), \dot{\theta}(t)] = 0$ since $\theta(t + T) = \theta(t)$. The remaining of the equation gives $\mathcal{W} = 0$.

indicates that the integral is computed along 1 period ($T = 2\pi/\Omega$) of the conservative solution θ_c perturbed at the order 2 to obtain a subharmonic resonance of the pendulum in the case of a parametric excitation. According to Eq. (23), the Melnikov function is rewritten such as

$$M^{1:2}(t) = w^{1:2}(\delta, t) - R(\mu_1, \mu_0), \tag{26}$$

where the first term corresponds to the work done by the parametric forcing along one period of the conservative solution and depends on the forcing amplitude such as

$$w^{1:2}(\delta, t) = -\,\delta \int_0^T \dot{\theta}_c(\tau + t)\, \cos 2\Omega\tau\, \theta_c(\tau + t)\, d\tau. \tag{27}$$

The second term of Eq. (26) corresponds to the dissipated energy along one period of the conservative solution due to viscous and dry friction and reads

$$R(\mu_1, \mu_0) = \int_0^T \dot{\theta}_c(\tau)\, \Big(\mu_1\, \dot{\theta}_c(\tau) + f_0(\dot{\theta}_c(\tau))\Big)\, d\tau. \tag{28}$$

This resistance term is independent of t since the friction terms do not explicitly depend on time. After calculations using the analytical solution θ_c of Eqs (17) and (18), Eqs. (27) and (28) become

$$\begin{cases} w^{1:2}(\delta, t) = W^{1:2}(\delta) \sin 2\Omega t & \text{(29a)} \\ R(\mu_1, \mu_0) = -\pi\mu_1\Omega a_c^2 - 4\mu_0 a_c & \text{(29b)} \end{cases}$$

with

$$W^{1:2}(\delta) = \frac{\pi}{2}\delta a_c^2\,. \tag{30}$$

The existence of solutions for the damped system forced at the frequency 2Ω with an amplitude δ can be stated according to Proposition 4.1 given in [6] and recalled here.

- $(\mathcal{P}_1)$: If $|W^{1:2}(\delta)| < |R(\mu_1, \mu_0)|$, no periodic solution persist.
- $(\mathcal{P}_2)$: If $|W^{1:2}(\delta)| = |R(\mu_1, \mu_0)|$, one periodic solution exists.
- $(\mathcal{P}_3)$: If $|W^{1:2}(\delta)| > |R(\mu_1, \mu_0)|$, two periodic solutions exist.

This proposition uses the balance of injected energy and dissipated energy to know if none, one or two periodic solutions exist for a given frequency. Examples of $(\mathcal{P}_1)$, $(\mathcal{P}_2)$ and $(\mathcal{P}_3)$ are presented in Figure 6 for a parametric oscillator with no dry friction and excited with a constant forcing displacement ($\delta = -4\Omega^2\tilde{\delta}$). Figure 6(a) is computed using Equations (29b) and (30) and Figure 6(b) is computed using Eq. (18) for the backbone curve a_c and Eq. (19) for the amplitude a of the parametric oscillator.

The curves representing the dissipated energy $|R|$ for $\mu_1 = 0.1$ (black line) and the injected energy $|W^{1:2}|$ for $\tilde{\delta}_1 = 0.015$ (yellow line) are plotted in Figure 6(a). It is noteworthy that these two curves never cross each other, which means that the injected energy is not sufficient enough to overcome the energy dissipated due to damping. Therefore, no periodic solution corresponding to $\tilde{\delta}_1 = 0.015$ is obtained in Figure 6(b). When increasing the forcing amplitude to $\tilde{\delta}_2 = 0.05$, which is the critical value computed using Eq. (21), the curves $|R|$ and $|W^{1:2}|$ (magenta line) cross each other at $\Omega = \omega_0$. This forcing amplitude correspond to the birth of the resonance represented by the magenta triangle in Figure 6(b). Then, the forced response of the system is plotted for $\tilde{\delta}_3 = 0.055$ (green line) in Figure 6(b). For the excitation frequency represented by the vertical black dashed line, no solution exist in this case. This can also be observed in Figure 6(a). Indeed, at the corresponding frequency (dashed vertical black line), the green curve representing

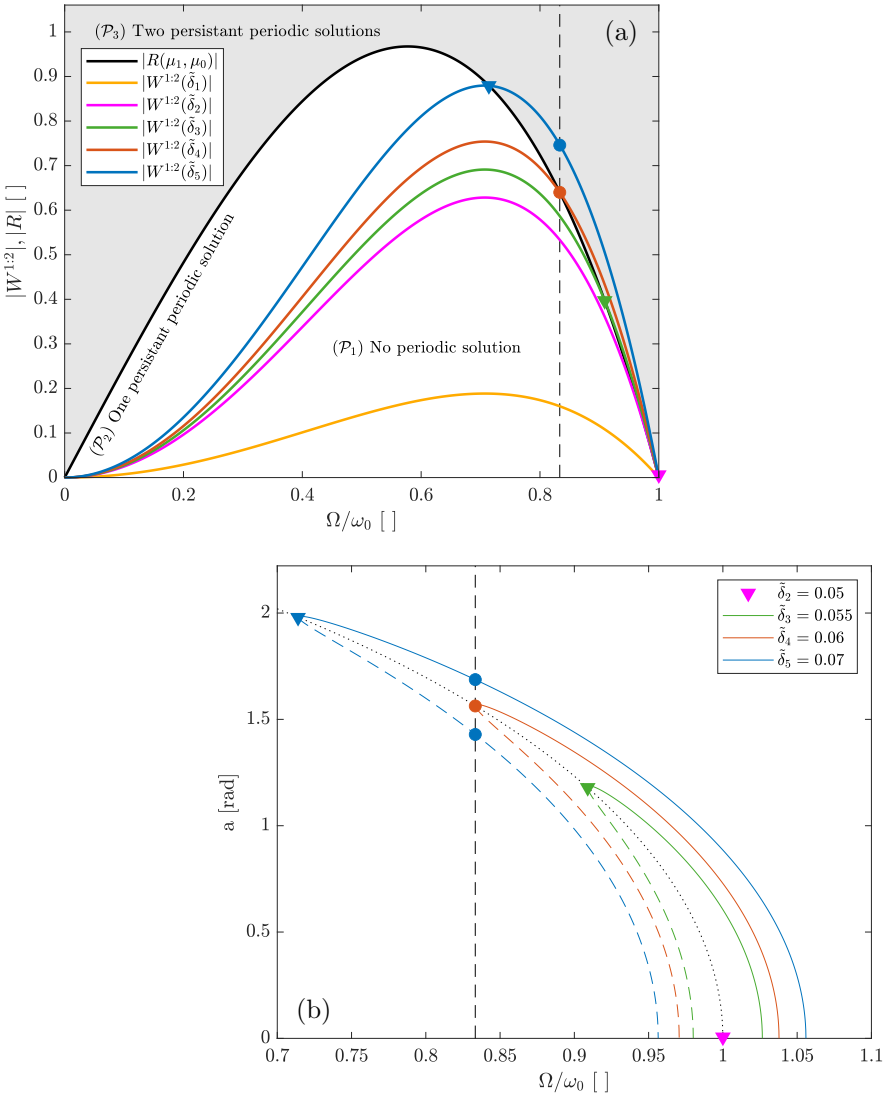

Fig. 6 Illustration of the method proposed in [6] and based on the energy principle. (a) Comparison between dissipated energy when $\mu_1 = 0.1$ and $\mu_0 = 0$ (plain black line) and injected energy for $\tilde{\delta}_1 = 0.015$ (yellow line), $\tilde{\delta}_2 = 0.05$ (magenta line), $\tilde{\delta}_3 = 0.055$ (green line), $\tilde{\delta}_4 = 0.06$ (red line) and $\tilde{\delta}_5 = 0.07$ (blue line). White and gray regions correspond respectively to propositions ($\mathcal{P}_1$) and ($\mathcal{P}_3$). The black plain line corresponds to the proposition ($\mathcal{P}_2$). (b) Corresponding forced responses of the system computed using the MVA. The dotted black line is the backbone curve corresponding to the conservative solution. Coloured bullets, triangles and the vertical dashed line are markers used to compared Figures (a) and (b).

the energy injected in the system by the forcing, does not cross, nor overcome the black plain line representing the energy dissipated by the system damping. According to ($\mathcal{P}_1$), no periodic solution exist at this frequency for these specific set of parameters. The forced response of the system for $\tilde{\delta}_4 = 0.06$ (red line) is then plotted in Figure 6(b). For the same excitation frequency, only one periodic solution exists represented by the red bullet. At the corresponding frequency

in Figure 6(a) (dashed vertical black line), the red curve representing the energy injected in the system by the forcing, crosses the black line representing the energy dissipated by the system damping. According to $(\mathcal{P}_2)$, only one periodic solution exists at this frequency for these specific set of parameters. Finally, the forced response of the system is plotted for $\tilde{\delta}_5 = 0.07$ in Figure 6(b) (blue line). In this case, two periodic solutions exist at the studied excitation frequency and are represented by blue bullets. In Figure 6(a), the blue curve is over the black line at this frequency where two periodic solutions exist for these specific set of parameters according to $(\mathcal{P}_3)$.

6.2 Estimation of the isola birth

For a pendulum without dry friction, the critical forcing amplitude is given by Eq. (21) and occurs at the critical frequency $\Omega_{cr} = \omega_0$ as presented in Section 3.3.3 and shown in Section 6.1. However, for a system including dry friction, the birth of isola observed in Figure 3 does not occur at ω_0 anymore. Therefore, it is necessary to find not only the critical forcing amplitude, but also at which critical frequency the birth of the isola occurs. With the assumption that the isola emerges from a point located on the backbone curve and for a constant forcing displacement excitation, it must exist a critical forcing amplitude $\tilde{\delta}_\Omega = \tilde{\delta}_{cr}$ which observes the proposition $(\mathcal{P}_2)$,

$$\left|\frac{\pi}{2}\ \delta\ a_c^2\right| = \left|-2\pi\ \Omega^2\ \tilde{\delta}_\Omega\ a_c^2\right| = \left|-\pi\mu_1\Omega a_c^2 - 4\mu_0 a_c\right| \ , \tag{31}$$

at the critical angular frequency $\Omega = \Omega_{cr}$. Using Eq. (18), the forcing amplitude $\tilde{\delta}_\Omega$, needed to obtain a single non trivial solution located on the backbone curve at Ω, reads

$$\tilde{\delta}_\Omega = \frac{\mu_1}{2\Omega} + \frac{2\mu_0}{\pi\Omega^2\sqrt{\frac{4}{3\gamma}(\omega_0^2 - \Omega^2)}} \ . \tag{32}$$

According to Proposition 4.3 in [6], the existence of a unique solution of Eq. (32) for any Ω can be detected when $\partial\tilde{\delta}_\Omega/\partial\Omega = 0$ and $\partial^2\tilde{\delta}_\Omega/\partial\Omega^2 > 0$. Indeed, since $\tilde{\delta}_\Omega$ is a convex function for $\Omega \in\ ]0, \omega_0[$, the angular frequency found with the two aforementioned conditions corresponds to the smallest value of $\tilde{\delta}_\Omega$ for a given set (μ_0, μ_1). This threshold value also corresponds to the critical forcing amplitude $\tilde{\delta}_{cr}$ which ensures that $|W^{1:2}|$ and $|R|$ are tangential. The condition on the first order derivative gives

$$\frac{\mu_1}{2}\Omega_{cr}(\omega_0^2 - \Omega_{cr}^2)^{3/2} = \frac{2\mu_0}{\pi}\sqrt{\frac{3\gamma}{4}}(3\Omega_{cr}^2 - 2\omega_0^2), \tag{33}$$

and is used to numerically compute the critical angular frequency Ω_{cr} also ensuring the validity of the condition on the second order derivative. Finally, the critical forcing amplitude $\tilde{\delta}_{cr}$ is computed injecting Ω_{cr} in Eq. (32).

Some remarks on this approach are made here. Firstly, it is noteworthy that Ω_{cr} is necessarily smaller than ω_0 (when $\tilde{\gamma} = 1/6$) since no real value of a_c exists for $\Omega > \omega_0$. Moreover, $a_c = 0$ when $\Omega = \omega_0$. Since $a = 0$ is not a solution of Eq. (13) when $\mu_0 \neq 0$, no intersection between non trivial solutions and the backbone curve can occur at the natural angular frequency ω_0 of the system. According to Eq. (33), it is stated again that $\Omega_{cr} = \omega_0$ for a system without dry friction. In this case, the critical forcing amplitude computed with Eq. (32) is the same as $\tilde{\delta}_{cr,(\mu_0=0)}$ presented in Section 3.3.3. For the special case $\mu_1 = 0$ and $\mu_0 \neq 0$, the critical angular frequency

does not depend on the value of the dry friction coefficient and is $\Omega_{cr} = \sqrt{2/3}\omega_0 \simeq 0.817\omega_0$. The corresponding critical forcing amplitude reads

$$\tilde{\delta}_{cr,(\mu_1=0)} = \frac{9\mu_0\sqrt{\tilde{\gamma}}}{2\pi\omega_0^2}\,. \tag{34}$$

A second remark is about the assumption that the isola birth occurs on the backbone curve. When the dry friction coefficient is not too large, Equations (33) and (32) give a good estimation of the critical angular frequency and amplitude. However, when the dry coefficient is large, the isola birth does not occur on the backbone curve as shown in Figures 3(c), (d) and 4(d). In this case, the proposed approach gives a less accurate approximation of the critical forcing amplitude and frequency.

6.3 Results

Cartographies of the critical forcing amplitude and angular frequency, respectively computed using Equations (32) and (33), are presented in Figure 7 for $\tilde{\gamma} = 1/6$ and $\omega_0 = 1$. These cartographies are useful to quickly determine what are the excitation force and frequency to obtain (or to avoid) a periodic motion for a parametric system including both dry and viscous damping.

Figure 7(a) shows that the relation between the damping coefficients and the critical forcing amplitude is roughly linear, with a greater influence for the dry friction coefficient. Since the surface shown in Figure 7(a) seems close to a plan, it is proposed to fit it with a two variables polynomial to obtain a simple analytical approximation of the critical forcing amplitude (see Appendix D). Figure 7(b) presents the corresponding critical angular frequency which variates between the two limits $\Omega_{cr,(\mu_0=0)} = \omega_0$ and $\Omega_{cr,(\mu_1=0)} = \sqrt{2/3}\,\omega_0$. The critical angular frequency quickly decreases toward $\Omega_{cr,(\mu_1=0)}$ when μ_0 increases showing again a great influence of the dry friction coefficient.

To further analyse the accuracy of the critical forcing amplitude and angular frequency estimation, some examples, identified with coloured markers and number k, are picked up from the cartographies of Figure 7. The corresponding damping parameters are given in Table 1. Figure

Table 1 Damping parameters used in examples presented in Figure 7.

k	1	2	3	4	5
μ_0	0.0024	0	0.0245	0.2449	0.2449
μ_1	0	0.05	0.1	0	0.1

8 presents illustrations of Propositions ($\mathcal{P}_2$) and ($\mathcal{P}_3$) and the corresponding MVA solutions for these few examples. In Figure 8(a), the method described in Section 6.1 is illustrated for a system including dry friction with the curves referred as $|R_4|$, $|R_5|$ and $|W_0^{1:2}|$ where the latter is computed with $\tilde{\delta} = 0.25$. The intersections between these resistance curves ($|R|$) and the curve related to the forcing ($|W^{1:2}|$) are represented by squares. In Figure 8(b), these markers correspond to the intersections between the non trivial solutions computed with the MVA and the backbone curve of the pendulum (plain black line). According to the proposition presented in Section 6.1, two solutions exist when $|W^{1:2}| > |R|$ (see ($\mathcal{P}_3$)) and only one solution exists when $|W^{1:2}| = |R|$ (see ($\mathcal{P}_2$)). Thus, the estimated birth of an isola in Figure 8(b) occurs when $|W^{1:2}|$ and $|R|$ are tangential in Figure 8(a). These cases are represented by coloured bullets (resp.

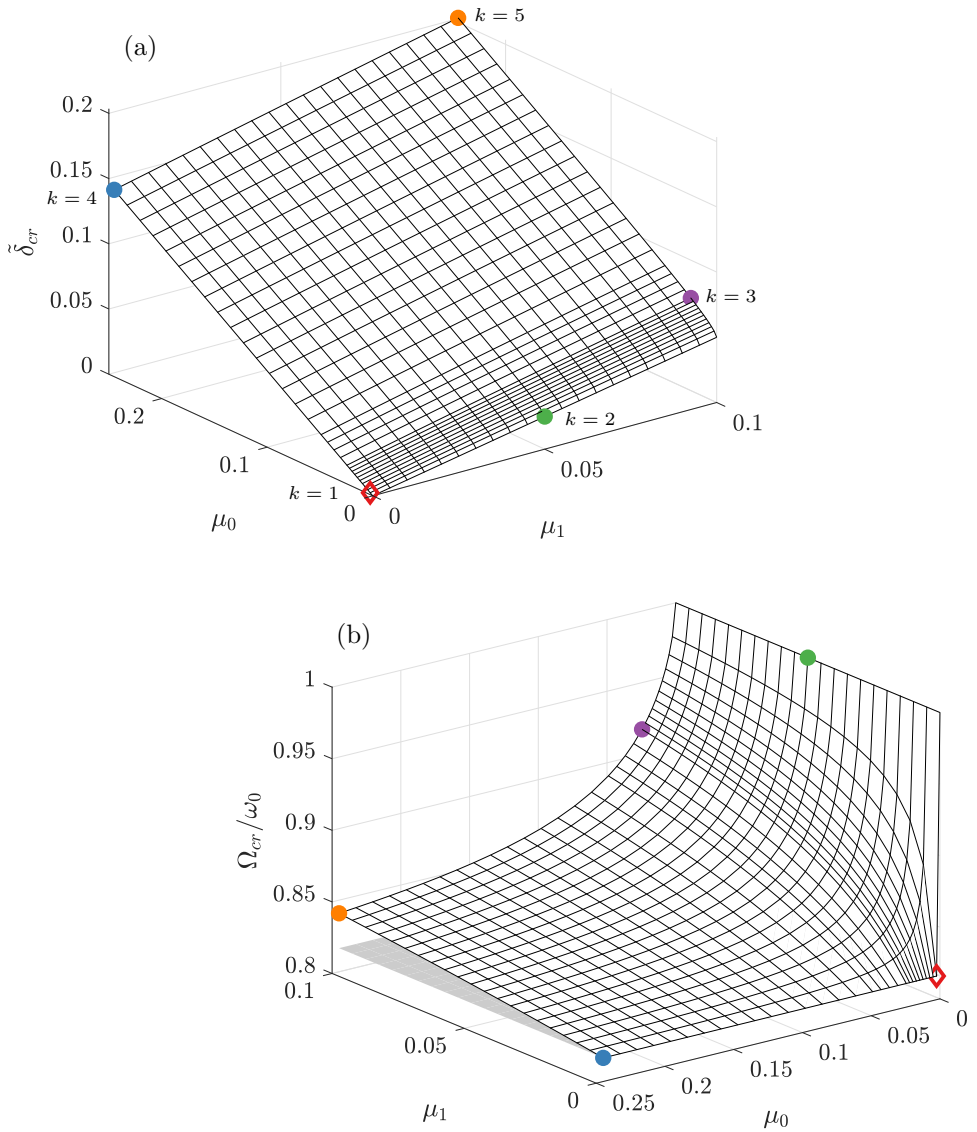

Fig. 7 Critical (a) forcing amplitude and (b) angular frequency as a function of μ_1 and μ_0. The horizontal gray plane in Figure 7(b) corresponds to $\Omega_{cr} = \sqrt{2/3}\,\omega_0$. Coloured markers correspond to examples presented in Figure 8 and denoted with the number k.

diamond) in Figure 8(a) for $k = 2, 5$ (resp. $k = 1$). As predicted in Section 6.2, the corresponding critical angular frequency is included in the interval $[\sqrt{2/3}\,\omega_0, \omega_0]$ represented by black dotted vertical lines for every k. Corresponding critical forcing amplitudes are used to compute the solutions of Eq. (13) which are plotted in Figure 8(b). For $k = 1$ (red diamond) and 2 (green circle), the birth of the isola occurs on the backbone curve. For $k = 3$ (purple circle), a small isola is tangential to the backbone when computed with the estimated critical forcing amplitude and angular frequency. For large values of μ_0, corresponding to $k = 4$ (blue circle) and 5 (yellow circle), it is clear that the estimated critical forcing amplitude does not correspond to the birth of

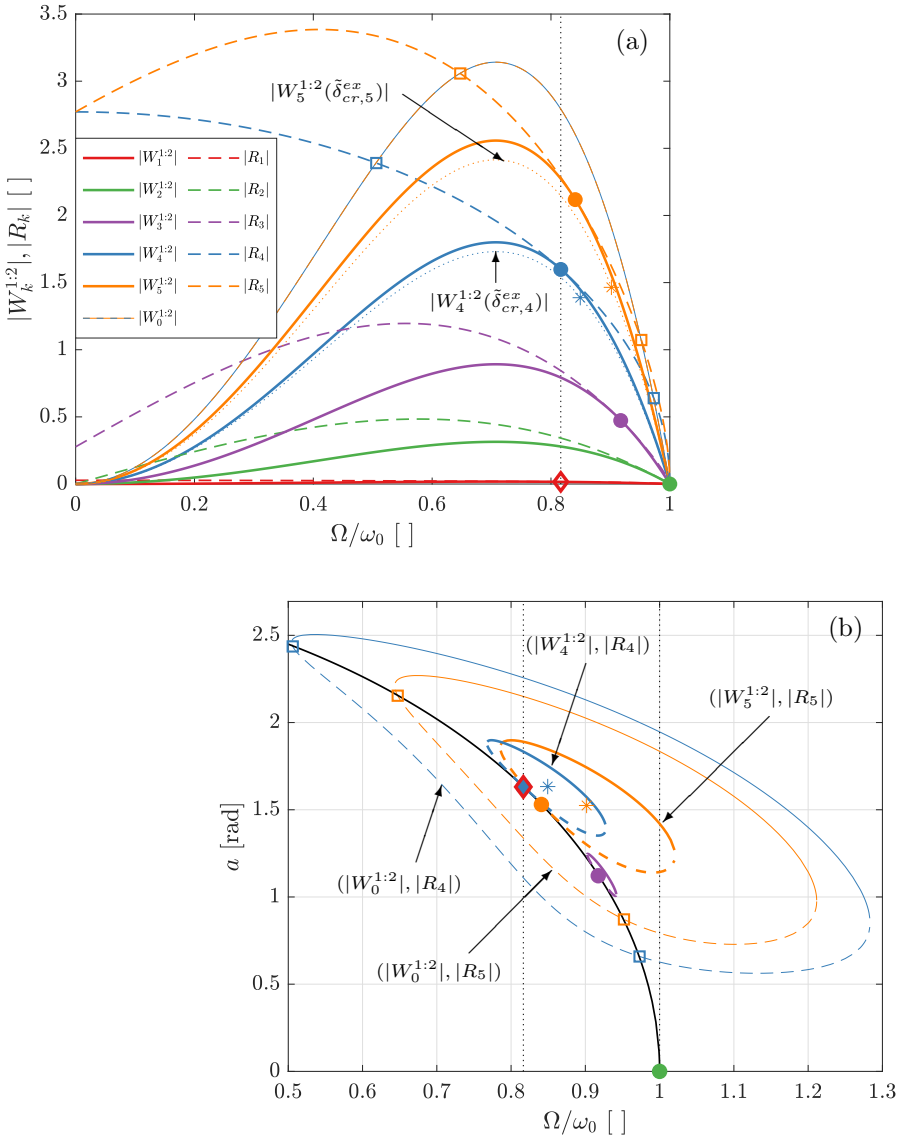

Fig. 8 (a) Energy principle illustrations using parameters drawn by coloured markers in Figure 7. $|W_k^{1:2}|$ is the maximum amplitude of the work done by the parametric forcing along one period of the pendulum conservative solution and $|R_k|$ is the resistance due to damping forces. $|W_0^{1:2}|$ is computed with $\tilde{\delta} = 0.25$. Bullet and diamond markers correspond to the estimated birth of non trivial solutions computed with Equations (32) and (33). For $k = 2$ and 5, dotted coloured lines correspond to $|W_k^{1:2}(\tilde{\delta}^{ex}_{cr,k})|$, where $\tilde{\delta}^{ex}_{cr,k}$ was manually tuned to obtain the exact birth of solutions represented by stars. (b) Corresponding stable and unstable solutions (respectively plain and dashed lines) computed using Eq. (13). Squares correspond to the intersections of the non trivial solutions with the conservative ones also indicated by the intersection of $|W_0^{1:2}|$ with $|R_4|$ and $|R_5|$ in Figure 8(a).

the isola. Instead, the isola computed using the MVA is tangential to the backbone curve. This is explained by the fact that the isola does not grow exactly around the backbone curve when μ_0 is large as seen in Figure 4(d). For $k = 4$ and 5, the exact critical forcing amplitude, denoted $\tilde{\delta}^{ex}_{cr,k}$,

is manually identified. The resulting curves $|W_k^{1:2}(\tilde{\delta}_{cr,k}^{ex})|$ are plotted in dotted coloured lines in Figure 8(a) and the corresponding isola birth are represented by stars in Figure 8(b). The exact critical forcing amplitude values are compared to the estimated ones in Table 2 which also gives the estimated and manually identified critical angular frequencies. The relative error between the forcing amplitudes are approximately 4% for $k = 4$ and 6% for $k = 5$. Similar relative errors are found between estimated and manually identified angular frequencies. Thus, for large values of μ_0, the proposed method does not give exactly the critical forcing amplitude and angular frequency due to the shift of the non trivial solutions around the backbone curve. As an interesting fact, the amplitudes at which isola emerges are almost the same when computed by the method based on the energy principle ($a_{cr,k}$) and manually identified ($a_{cr,k}^{ex}$). These values are also given in Table 2 and the relative errors between them are less than 0.5%.

Table 2 Critical forcing amplitude and angular frequency estimated with Equations (32) and (33) and manually identified for $k = 4$ and 5.

k	$\tilde{\delta}_{cr,k}$	$\tilde{\delta}_{cr,k}^{ex}$	$\Omega_{cr,k}$	$\Omega_{cr,k}^{ex}$	$a_{cr,k}$	$a_{cr,k}^{ex}$
4	0.1432	0.1377	0.8165	0.8493	1.631	1.633
5	0.2035	0.1921	0.8408	0.9017	1.530	1.525

7 Conclusion

This paper addresses the effect of dry friction on the dynamical behaviour of a parametric non linear oscillator. The example of a parametrically excited pendulum including viscous and dry friction is studied. The theoretical solutions of the system are derived using the harmonic balance method. The stability of obtained non trivial solutions is studied using the method of varying amplitude. Since the perturbation method used in this paper does not allow the computation of trivial solutions for the case including dry friction, the existence and stability of the motionless solutions of the system are studied using time integration simulations. To avoid the linearisation of the dry friction term during these simulations, a switch model is used for the modelling.

When including dry friction, it was found that the trivial solutions of the system always exist and are always stable. Non trivial solutions also exist but are isolated from the trivial solutions compared to the case with no dry friction. The dry friction also has the effect to shift the birth of these isola from the conservative solutions of the system. Thus, isola do not emerge form the backbone curve and it is possible to obtain non trivial solutions which never cross the backbone curve when the dry friction coefficient is very large. The effects of the system initial conditions on the basins of attraction of the isolated non trivial solutions are investigated using time integration simulations. It is found that the initial angular displacement impose to the pendulum and its initial phase with the parametric excitation must be carefully chosen to obtain the largest basin of attraction of the isolated solutions. Moreover, the initial angular displacement must also exceed a threshold value to initiate the motion of the pendulum due to the stability of trivial solutions. Finally, a method to estimate the critical forcing amplitude needed to jump on the non trivial solutions stable branch is proposed using an approach based on the energy principle. The corresponding critical angular frequency is also derived from this approach. The proposed method gives a relevant estimation of these force and frequency for small values of the dry friction coefficient. When the latter are large, the computed critical values are not exact due to the shift of the non trivial solutions from the conservative solution of the system.

Future works must address the correction of the energy principle approach to better estimate the critical forcing amplitude and angular frequency. The manner to precisely impose initial conditions to a parametric pendulum must also be further investigated.

A Solutions of the equation of motion using the method of multiple scales

To use the method of multiple scales (MMS), Eq. (5) is rewritten using ϵ as a bookkeeping parameter to identify small terms such as

$$\ddot{\theta} + \epsilon\mu_1\dot{\theta} + \epsilon f_0(\dot{\theta}) + [\omega_0^2 + \epsilon\delta\cos 2\Omega t]\theta - \epsilon\gamma\theta^3 = 0. \tag{35}$$

The solutions of Eq. (35) are calculated using the expansion

$$\theta(t,\epsilon) = \theta_0(T_0,T_1) + \epsilon\theta_1(T_0,T_1) + O(\epsilon^2), \tag{36}$$

with $T_0 = t$ and $T_1 = \epsilon t$ fast and slow independent time scale respectively. Substituting this expansion into Eq. (35) and equating to zero the coefficients of orders ϵ^0 and ϵ^1 yields

$$\begin{cases} D_0^2\theta_0 + \omega_0^2\theta_0 = 0 \\ D_0^2\theta_1 + \omega_0^2\theta_1 = -2D_0D_1\theta_0 - \mu_1 D_0\theta_0 - f_0(D_0\theta_0) - \delta\cos 2\Omega t\theta_0 + \gamma\theta_0^3 \end{cases} \tag{37}$$

with $D_n^i = \partial^i/\partial T_n^i$ partial differential operators. Using $i = \sqrt{-1}$ and $^-$ denoting the complex conjugate, the solution of the first equation of the system (37) can be written in the form

$$\theta_0 = A(T_1)e^{i\,\omega_0\,T_0} + \bar{A}(T_1)e^{-i\,\omega_0\,T_0}. \tag{38}$$

Substituting this solution in the second equation of the System (37) gives

$$\begin{aligned} D_0^2\,\theta_1 + \omega_0^2\,\theta_1 = & \left[-2i\omega_0\,D_1A - i\omega_0\mu_1\,A + 3\gamma\,A^2\bar{A}\right]\,e^{i\,\omega_0\,T_0} \\ & - \tfrac{\delta}{2}\,\left[Ae^{i(\omega_0+2\Omega)T_0} + \bar{A}e^{-i(\omega_0-2\Omega)T_0}\right] \\ & + \gamma\,A^3\,e^{i3\omega_0T_0} + \;cc\; - f_0(i\omega_0Ae^{i\omega_0T_0} - i\omega_0\bar{A}e^{-i\omega_0T_0}) \end{aligned} \tag{39}$$

where cc denotes complex conjugate terms.

In order to investigate the primary parametric resonance of the system, the case $\Omega \approx \omega_0$ is studied introducing a detuning parameter σ such as

$$\Omega = \omega_0 + \epsilon\frac{\sigma}{2}. \tag{40}$$

Eq. (39) becomes

$$\begin{aligned} D_0^2\theta_1 + \omega_0^2\,\theta_1 = & \left[-2i\omega_0\,D_1A - i\omega_0\mu_1\,A + 3\gamma\,A^2\bar{A}\right]\,e^{i\,\omega_0\,T_0} - \tfrac{\delta}{2}\,\left[Ae^{i3\omega_0T_0} + \bar{A}e^{i\omega_0T_0}\right]e^{i\sigma T_1} \\ & + \gamma\,A^3\,e^{i3\omega_0T_0} + \;cc\; - f_0(i\omega_0Ae^{i\omega_0T_0} - i\omega_0\bar{A}e^{-i\omega_0T_0}) \end{aligned} \tag{41}$$

At this stage, the method of multiple scales has the advantage to clearly reveal the resonant terms (depending on $e^{i\,\omega_0\,T_0}$) responsible for secular terms in the solutions of θ_1. To capture all the resonant terms, the dry friction function can be expanded in a Fourier series

$$f_0(i\omega_0\,Ae^{i\omega_0T_0} - i\omega_0\,\bar{A}e^{-i\omega_0T_0}) = \sum_{-\infty}^{+\infty} c_n\;e^{in\omega_0T_0} \tag{42}$$

with c_n the Fourier coefficients such as

$$c_n = \frac{\omega_0}{2\pi}\int_0^{2\pi/\omega_0} f_0(i\omega_0Ae^{i\omega_0T_0} - i\omega_0\bar{A}e^{-i\omega_0T_0})\;e^{-in\omega_0T_0}dT_0. \tag{43}$$

Thus, the only resonant term of the Fourier series (42) is $c_1\;e^{i\omega_0T_0}$.

To eliminate secular terms, the resonant terms in Eq. (41) must vanish giving the solvability condition

$$-2i\omega_0\,D_1A - i\omega_0\mu_1\,A + 3\gamma\,A^2\bar{A} - \frac{\delta}{2}\,\bar{A}\,e^{i\sigma T_1} - c_1 = 0 \tag{44}$$

Then, the polar form $A = \frac{1}{2} a_{ms} e^{ib}$ is introduced to be able to separate real and imaginary parts of the solvability condition. This yields $D_1 A = \frac{1}{2}(a'_{ms} + i a_{ms} b') e^{ib}$ where $'$ denotes the derivative with respect to T_1. A new parameter is also introduced such as $\phi = \omega_0 T_0 + b$ leading to the new form $\theta_0 = a_{ms} \cos\phi$. Using these notations and considering the case $a_{ms} > 0$, the dry friction term reads

$$c_1 = \frac{1}{2\pi} \int_0^{2\pi} f_0(-a_{ms}\omega_0 \ \sin\phi) \ e^{-i\phi} \ e^{ib} \ d\phi = \frac{2i\mu_0}{\pi} e^{ib} \tag{45}$$

and the solvability condition becomes

$$\left[-i\omega_0 \left(a'_{ms} + i a_{ms} b'\right) - \frac{i\omega_0 \mu_1}{2} \, a_{ms} + \frac{3\gamma}{8} \, a_{ms}^3 - \frac{\delta}{4} \, a_{ms} \, e^{i2(\frac{\sigma}{2} T_1 - b)} - \frac{2i\mu_0}{\pi} \right] \ e^{ib} = 0. \tag{46}$$

The system of modulation equations is obtained separating real and imaginary parts of Eq. (46) and reads

$$\begin{cases} a'_{ms} \quad = -\frac{\mu_1}{2} \, a_{ms} - \frac{\delta}{4\omega_0} \, a_{ms} \ \sin 2(\frac{\sigma}{2} T_1 - b) - \frac{2\mu_0}{\pi\omega_0} \\ a_{ms} b' = -\frac{3\gamma}{8\omega_0} \, a_{ms}^3 + \frac{\delta}{4\omega_0} \, a_{ms} \ \cos(2(\frac{\sigma}{2} T_1 - b)) \end{cases} \tag{47}$$

Using $\psi = \frac{\sigma}{2} T_1 - b$ to make the system autonomous (no explicit term in T_1), the modulation equations become

$$\begin{cases} a'_{ms} \quad = -\frac{\mu_1}{2} \, a_{ms} - \frac{2\mu_0}{\pi\omega_0} - \frac{\delta}{4\omega_0} \, a_{ms} \ \sin 2\psi \\ a_{ms} \psi' = \frac{\sigma}{2} \, a_{ms} + \frac{3\gamma}{8\omega_0} \, a_{ms}^3 - \frac{\delta}{4\omega_0} \, a_{ms} \ \cos 2\psi \end{cases} \tag{48}$$

To find the fixed points of the system, the amplitude and phase are searched such as $a'_{ms} = \psi' = 0$. Thus, the system (48) gives

$$\left(\frac{\delta}{4\omega_0} \right)^2 a_{ms}^2 = \left(\frac{\mu_1}{2} \, a_{ms} + \frac{2\mu_0}{\pi\omega_0} \right)^2 + \left(\frac{\sigma}{2} \, a_{ms} + \frac{3\gamma}{8\omega_0} \, a_{ms}^3 \right)^2 \tag{49}$$

Developing this equation gives a 6^{th} degree polynomial equation such as

$$\frac{9}{16} \, \gamma^2 \, a_{ms}^6 + \frac{3}{2} \, \gamma \, \omega_0 \sigma \, a_{ms}^4 + \left(\omega_0^2 \sigma^2 + \omega_0^2 \mu_1^2 - \frac{1}{4} \, \delta^2 \right) \, a_{ms}^2 + \frac{8}{\pi} \, \omega_0 \mu_0 \mu_1 \ a_{ms} + \frac{16}{\pi^2} \, \mu_0^2 = 0. \tag{50}$$

For ψ the solution reads

$$\tan(2\psi) = -\frac{\omega_0 \, \mu_1 \, a_{ms} + \frac{4}{\pi} \, \mu_0}{\omega_0 \sigma \, a_{ms} + \frac{3}{4} \, \gamma \, a_{ms}^3} \, . \tag{51}$$

The stability of non trivial solutions is computed using the Jacobian of the modulation equations (48) which reads

$$J(a_{ms}, \psi) = \begin{bmatrix} \frac{\partial a'_{ms}}{\partial a_{ms}} & \frac{\partial a'_{ms}}{\partial \psi} \\ \frac{\partial \psi'}{\partial a_{ms}} & \frac{\partial \psi'}{\partial \psi} \end{bmatrix} = \begin{bmatrix} -\frac{\mu_1}{2} - \frac{\delta}{4\omega_0} \sin 2\psi & -\frac{\delta}{2\omega_0} \, a_{ms} \ \cos 2\psi \\ \frac{3\gamma}{4\omega_0} \, a_{ms} & \frac{\delta}{2\omega_0} \ \sin 2\psi \end{bmatrix} \tag{52}$$

The condition for stability of solutions is given by the real part of the Jacobian eigenvalues $\lambda(\omega)$. When $Re(\lambda(\omega)) < 0$ solutions are stable and unstable otherwise.

Solutions obtained using the method of multiple scales are compared to those computed with the method of varying amplitude presented in Section 3.1 for the special case $\mu_0 = 0$. To evaluate the precision of both methods, the asymptotic numerical method (ANM) using a harmonic balance method with eleven harmonics implemented in the Manlab code is used as reference [14]. Results are computed for a constant forcing displacement ($\delta = -4\Omega^2\tilde{\delta}$) and a constant forcing acceleration ($\delta = \tilde{\delta}_a$) defined to have the same amplitude at $\Omega = 1$ and for γ both positive and negative. The amplitudes of the first harmonic for MVA and ANM and of the first expansion term for MMS are plotted in Figure 9. It has been verified that the amplitude of the first harmonic for the ANM is similar to the amplitude norm computed using the eleven harmonics.

The first point about these results is that the MVA gives more accurate solutions than MMS. The MVA gives globally good results compared to the ANM solutions except in the case of the constant forcing acceleration (see Fig. 9(b)) and a softening behaviour ($\gamma = 1/6$). In this case, the non trivial solutions predicted by the MVA have no low frequency bound unlike for the ANM solutions. Moreover, the stability of the higher branch of the solutions is not well predicted by the MVA compared to the ANM solutions.

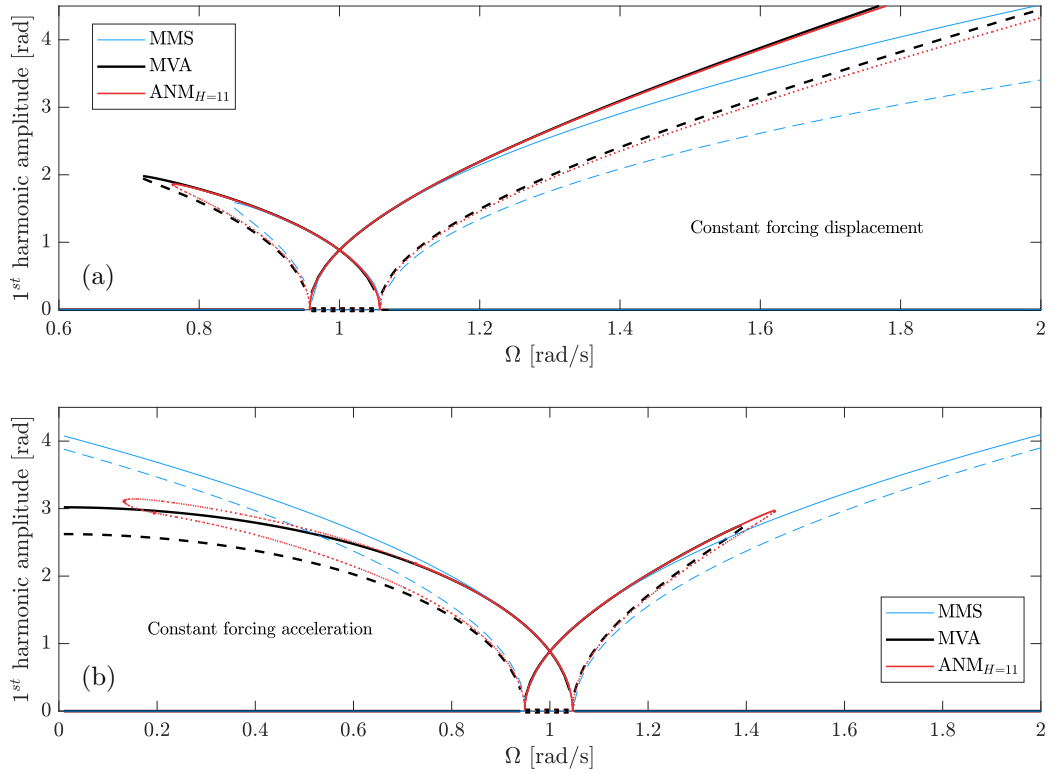

Fig. 9 Comparison between the method of multiple scales (blue), method of varying amplitude (black) and asymptotic numerical method using harmonic balance method (red) for (a) a constant forcing displacement ($\delta = -0.28\,\Omega^2$) and (b) a constant forcing acceleration ($\delta = -0.28$). The softening behaviour (tilt toward low frequencies) is obtained for $\gamma = 1/6$ and the hardening behaviour (tilt toward high frequencies) for $\gamma = -1/6$. Other parameters are $\mu_1 = 0.1$, $\mu_0 = 0$, $\omega_0 = 1$. Plain and dashed or dotted curves respectively correspond to stable and unstable solutions.

The second point about these results is that the form of the forcing amplitude (constant displacement or acceleration) modifies the behaviour of the system. Indeed, for a softening behaviour ($\gamma = 1/6$), a low frequency bound is predicted by analytical methods for non trivial solutions when a constant forcing displacement is applied but not for a constant forcing acceleration. On the contrary, for a hardening behaviour ($\gamma = -1/6$), a high frequency bound is predicted by the ANM and the MVA when a constant forcing acceleration is applied. In this case, the MMS failed to predict this solution bound as presented in [1]. This justifies the choice of the MVA in this article instead of MMS.

B Rewriting of the governing equation with three dependent parameters

In order to reduce the number of dependent parameters in the equation of motion, Eq. (5) is rewritten using the following variables

$$\hat{\theta} = \sqrt{\tilde{\gamma}}\theta, \quad \hat{t} = \omega_0 t, \tag{53}$$

and parameters

$$\hat{\Omega} = \frac{\Omega}{\omega_0}, \quad \hat{\mu}_1 = \frac{\mu_1}{\omega_0}, \quad \hat{\mu}_0 = \frac{\mu_0\sqrt{\tilde{\gamma}}}{\omega_0^2} \tag{54}$$

and reads

$$\ddot{\hat{\theta}} + \hat{\mu}_1\dot{\hat{\theta}} + \hat{f}_0(\dot{\hat{\theta}}) + (1 - 4\hat{\Omega}^2\tilde{\delta}\cos 2\hat{\Omega}\hat{t})\hat{\theta} - \hat{\theta}^3 = 0, \tag{55}$$

with $\hat{f}_0(\dot{\hat{\theta}})$ equals $f_0(\dot{\hat{\theta}})$ as defined in Eq. (3) substituting μ_0 with $\hat{\mu}_0$. Thus, solutions of Eq. (55) depend on the three parameters $\tilde{\delta}$, $\hat{\mu}_0$ and $\hat{\mu}_1$ only.

C Details on the MVA developments

The derivatives of the expansion presented in Section 3.1 read

$$\begin{cases} \dot{\theta} = \dot{a}\cos\Phi - a(\Omega+\dot{\beta})\sin\Phi \\ \\ \ddot{\theta} = (\ddot{a} - a(\Omega+\dot{\beta})^2)\cos\Phi - (2\dot{a}(\Omega+\dot{\beta}) + a\ddot{\beta})\sin\Phi \end{cases} \tag{56}$$

and non linear and parametric terms of Eq. (5) read

$$\begin{cases} \theta^3 &= \frac{1}{4}a^3(3\cos\Phi + \cos 3\Phi) \\ \\ \cos(2\Omega t)\theta &= \frac{1}{2}a[\cos 2\beta(\cos\Phi + \cos 3\Phi) + \sin 2\beta(\sin\Phi + \sin 3\Phi)] \end{cases} \tag{57}$$

D Analytical estimation of the critical forcing amplitude

The critical forcing amplitude map computed in Section 6.3 and presented in Figure 7(a) is fitted using a regression with an order 4 polynomial in μ_0 and 1 in μ_1.

$$\tilde{\delta}_{cr}^{pol}(\mu_1,\mu_0) = c_{10}\,\mu_1 + c_{01}\,\mu_0 + c_{11}\,\mu_1\,\mu_0 + c_{02}\,\mu_0^2 + c_{12}\,\mu_1\,\mu_0^2 + c_{03}\,\mu_0^3 + c_{13}\,\mu_1\,\mu_0^3 + c_{04}\,\mu_0^4 \tag{58}$$

The computed coefficient of determination is $R^2 = 0.9999$ and the final root mean square error is $RMSE = 0.0009204$. The coefficients of the polynomial are given in Table 3. To evaluate the accuracy of the polynomial,

Table 3 Coefficients of the polynomial fitting the critical forcing amplitude computed in Section 6.3.

c_{10}	c_{01}	c_{11}	c_{02}	c_{12}	c_{03}	c_{13}	c_{04}
0.5027	0.601	2.757	-0.3691	-21.78	2.571	51.08	-5.498

the relative error between the critical forcing amplitude presented in Figure 7(a) and the values obtained with Eq. (58) is given in Figure 10. The polynomial described by Eq. (58) and Table 3 gives an acceptable approximation of the critical forcing amplitude since the relative error computed in Figure 10 is smaller than 8% for all considered values of μ_1 and μ_0. Notice that the relative error is not computed for $\mu_1 = \mu_0 = 0$ since $\tilde{\delta}_{cr}$ equals zero for these parameters. Since Polynomial (58) has no constant term, $\tilde{\delta}_{cr}^{pol}$ also equals zero for these set of parameters.

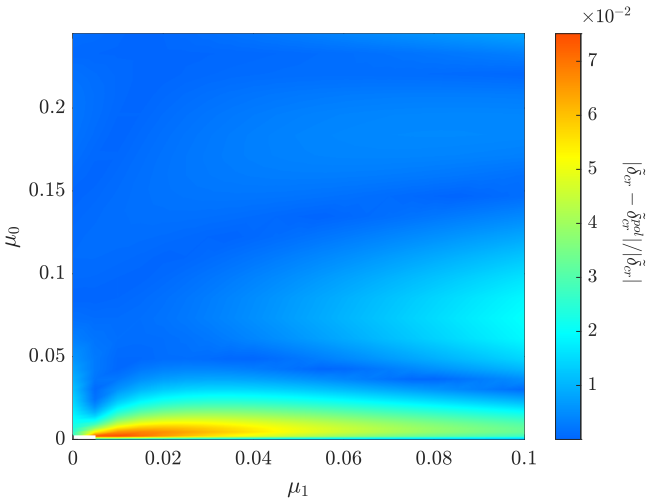

Fig. 10 Relative error between the critical forcing amplitude computed in Section 6.3 and approximated with the polynomial (58) as a function of μ_1 and μ_0.

Funding

Not applicable

Conflict of interest

The authors declare that they have no conflict of interest.

Availability of data and material

Not applicable

Code availability

All parameters used to compute the presented results are given in the paper.

References

1. Aghamohammadi, M., Sorokin, V., Mace, B.: On the response attainable in nonlinear parametrically excited systems. Applied Physics Letters **115**(15), 154102 (2019). DOI 10.1063/1.5120434. URL https://aip.scitation.org/doi/10.1063/1.5120434
2. Bertrand, C., Ture Savadkoohi, A., Lamarque, C.H.: Nonlinear oscillations of a pendulum cable with the effects of the friction and the radius of the support. Nonlinear Dynamics **96**(2), 1303–1315 (2019). DOI 10.1007/s11071-019-04854-5. URL http://link.springer.com/10.1007/s11071-019-04854-5
3. Bishop, S.R., Clifford, M.J.: Zones of chaotic behaviour in the parametrically excited pendulum. Zones of chaotic behaviour in the parametrically excited pendulum **189**(1), 142–147 (1996)

4. Bryant, P.J., Miles, J.W.: On a periodically forced, weakly damped pendulum. Part 3: Vertical forcing. The ANZIAM Journal **32**(1), 42–60 (1990). DOI 10.1017/S0334270000008201. URL https://www.cambridge.org/core/journals/anziam-journal/article/on-a-periodically-forced-weakly-damped-pendulum-part-3-vertical-forcing/C279AA663F76676EBA3C7D527A79E633
5. Butikov, E.I.: Spring pendulum with dry and viscous damping. Communications in Nonlinear Science and Numerical Simulation **20**(1), 298–315 (2015). DOI 10.1016/j.cnsns.2014.04.026. URL http://www.sciencedirect.com/science/article/pii/S1007570414002111
6. Cenedese, M., Haller, G.: How do conservative backbone curves perturb into forced responses? A Melnikov function analysis. Proceedings of the Royal Society A: Mathematical, Physical and Engineering Sciences **476**(2234), 20190494 (2020). DOI 10.1098/rspa.2019.0494. URL https://royalsocietypublishing.org/doi/10.1098/rspa.2019.0494
7. Cheng, G., Zu, J.W.: A numerical study of a dry friction oscillator with parametric and external excitations. Journal of Sound and Vibration **287**(1-2), 329–342 (2005). DOI 10.1016/j.jsv.2004.11.003. URL https://linkinghub.elsevier.com/retrieve/pii/S0022460X04008892
8. Daqaq, M.F., Stabler, C., Qaroush, Y., Seuaciuc-Osório, T.: Investigation of power harvesting via parametric excitations. Journal of Intelligent Material Systems and Structures (2008). DOI 10.1177/1045389X08100978. URL https://journals.sagepub.com/doi/10.1177/1045389X08100978
9. De Paula, A.S., Savi, M.A., Vaziri, V., Pavlovskaia, E., Wiercigroch, M.: Experimental bifurcation control of a parametric pendulum. Journal of Vibration and Control **23**(14), 2256–2268 (2017). DOI 10.1177/1077546315613237. URL http://journals.sagepub.com/doi/10.1177/1077546315613237
10. Denis, V., Jossic, M., Giraud-Audine, C., Chomette, B., Renault, A., Thomas, O.: Identification of nonlinear modes using phase-locked-loop experimental continuation and normal form. Mechanical Systems and Signal Processing **106**, 430–452 (2018). DOI 10.1016/j.ymssp.2018.01.014. URL https://www.sciencedirect.com/science/article/pii/S0888327018300220
11. Feeny, B.F., Liang, J.W.: A decrement method for the simultaneous estimation of coulomb and viscous friction. Journal of Sound and Vibration **195**(1), 149–154 (1996). DOI 10.1006/jsvi.1996.0411. URL http://www.sciencedirect.com/science/article/pii/S0022460X96904113
12. Galchev, T., Aktakka, E.E., Najafi, K.: A piezoelectric parametric frequency increased generator for harvesting low-frequency vibrations. Journal of Microelectromechanical Systems **21**(6), 1311–1320 (2012). DOI 10.1109/JMEMS.2012.2205901. URL http://ieeexplore.ieee.org/document/6251992/
13. Gonzalez-Buelga, A., Wagg, D.J., Neild, S.A.: Parametric variation of a coupled pendulum-oscillator system using real-time dynamic substructuring. Structural Control and Health Monitoring **14**(7), 991–1012 (2007). DOI 10.1002/stc.189. URL http://doi.wiley.com/10.1002/stc.189
14. Guillot, L., Lazarus, A., Thomas, O., Vergez, C., Cochelin, B.: A purely frequency based Floquet-Hill formulation for the efficient stability computation of periodic solutions of ordinary differential systems. Journal of Computational Physics **416**, 109477 (2020). DOI 10.1016/j.jcp.2020.109477. URL https://linkinghub.elsevier.com/retrieve/pii/S0021999120302515
15. Hartog, J.P.D.: LXXIII. Forced vibrations with combined viscous and coulomb damping. The London, Edinburgh, and Dublin Philosophical Magazine and Journal of Science **9**(59), 801–817 (1930). DOI 10.1080/14786443008565051. URL https://doi.org/10.1080/14786443008565051
16. Hill, T., Cammarano, A., Neild, S., Wagg, D.: Interpreting the forced responses of a two-degree-of-freedom nonlinear oscillator using backbone curves. Journal of Sound and Vibration **349**, 276–288 (2015). DOI 10.1016/j.jsv.2015.03.030. URL https://linkinghub.elsevier.com/retrieve/pii/S0022460X15002485
17. Hinrichs, N., Oestreich, M., Popp, K.: On the modelling of friction oscillators. Journal of Sound and Vibration **216**(3), 435–459 (1998)
18. Horton, B., Wiercigroch, M., Xu, X.: Transient tumbling chaos and damping identification for parametric pendulum. Philosophical Transactions of the Royal Society A: Mathematical, Physical and Engineering Sciences **366**(1866), 767–784 (2008). DOI 10.1098/rsta.2007.2126. URL https://royalsocietypublishing.org/doi/10.1098/rsta.2007.2126
19. Leine, R., van Campen, D., de Kraker, A., van den Steen, L.: Stick-Slip Vibrations Induced by Alternate Friction Models. Nonlinear Dynamics **16**(1), 41–54 (1998). DOI 10.1023/A:1008289604683. URL https://doi.org/10.1023/A:1008289604683
20. Leine, R.I., Nijmeijer, H.: Dynamics and Bifurcations of Non-Smooth Mechanical Systems. Springer (2004)
21. Nayfeh, A.H., Balachandran, B.: Applied Nonlinear Dynamics: Analytical, Computational, and Experimental Methods, 1 edn. Wiley (1995). DOI 10.1002/9783527617548. URL https://onlinelibrary.wiley.com/doi/book/10.1002/9783527617548
22. Nayfeh, A.H., Mook, D.T.: Nonlinear oscillations. John Wiley & sons, inc., New-York (1979)
23. de Paula, A.S., Savi, M.A., Pereira-Pinto, F.H.I.: Chaos and transient chaos in an experimental nonlinear pendulum. Journal of Sound and Vibration **294**(3), 585–595 (2006). DOI 10.1016/j.jsv.2005.11.015. URL https://linkinghub.elsevier.com/retrieve/pii/S0022460X05007303
24. Rugar, D., Grütter, P.: Mechanical parametric amplification and thermomechanical noise squeezing. Physical Review Letters **67**(6), 699–702 (1991). DOI 10.1103/PhysRevLett.67.699. URL https://link.aps.org/doi/10.1103/PhysRevLett.67.699

25. Shampine, L.F., Reichelt, M.W.: he matlab ode suite. SIAM Journal on Scientific Computing **18**, 1–22 (1997)
26. Shoeybi, M., Ghorashi, M.: Nonlinear Vibration Control of a System with Dry Friction and Viscous Damping Using the Saturation Phenomenon. Nonlinear Dynamics **45**(3), 249–272 (2006). DOI 10.1007/s11071-006-1438-2. URL https://doi.org/10.1007/s11071-006-1438-2
27. Sorokin, V.S., Thomsen, J.J.: Vibration suppression for strings with distributed loading using spatial cross-section modulation. Journal of Sound and Vibration **335**, 66–77 (2015). DOI 10.1016/j.jsv.2014.09.028. URL https://linkinghub.elsevier.com/retrieve/pii/S0022460X14007585
28. Surappa, S., Satir, S., Degertekin, F.L.: A capacitive ultrasonic transducer based on parametric resonance. Applied Physics Letters **111**, 043503 (2017)
29. Thomas, O., Mathieu, F., Mansfield, W., Huang, C., Trolier-McKinstry, S., Nicu, L.: Efficient parametric amplification in micro-resonators with integrated piezoelectric actuation and sensing capabilities. Applied Physics Letters **102**(16), 163504 (2013). DOI 10.1063/1.4802786. URL https://aip.scitation.org/doi/10.1063/1.4802786
30. Thomsen, J.J.: Vibrations and stability: advanced theory, analysis, and tools, 2nd ed edn. Springer, Berlin ; New York (2003)
31. Vakilinejad, M., Grolet, A., Thomas, O.: A comparison of robustness and performance of linear and nonlinear Lanchester dampers. Nonlinear Dynamics **100**(1), 269–287 (2020). DOI 10.1007/s11071-020-05512-x. URL https://doi.org/10.1007/s11071-020-05512-x
32. Vidmar, B.J., Feeny, B.F., Shaw, S.W., Haddow, A.G., Geist, B.K., Verhanovitz, N.J.: The effects of Coulomb friction on the performance of centrifugal pendulum vibration absorbers. Nonlinear Dynamics **69**(1), 589–600 (2012). DOI 10.1007/s11071-011-0289-7. URL https://doi.org/10.1007/s11071-011-0289-7
33. Xu, X., Wiercigroch, M.: Approximate analytical solutions for oscillatory and rotational motion of a parametric pendulum. Nonlinear Dynamics **47**(1-3), 311–320 (2006). DOI 10.1007/s11071-006-9074-4. URL http://link.springer.com/10.1007/s11071-006-9074-4
34. Yabuno, H., Murakami, T., Kawazoe, J., Aoshima, N.: Suppression of Parametric Resonance in Cantilever Beam With a Pendulum (Effect of Static Friction at the Supporting Point of the Pendulum). Journal of Vibration and Acoustics **126**(1), 149–162 (2004). DOI 10.1115/1.1596554. URL https://asmedigitalcollection.asme.org/vibrationacoustics/article/126/1/149/463517/Suppression-of-Parametric-Resonance-in-Cantilever
35. Yano, S.: Parametric Excitation in the Self-excited Vibration System with Dry Friction : 1st Report, Parametric Resonance. Bulletin of JSME **27**(224), 255–262 (1984). DOI 10.1299/jsme1958.27.255